Electronic Supplementary Material for "Vulnerability of Existing and Planned Coal-Fired Power Plants in Developing Asia to Changes in Climate and Water Resources"

Yaoping Wang,*[abc] Edward Byers,[b] Simon Parkinson,[bd] Niko Wanders,[e] Yoshihide Wada[b], Jiafu Mao,[f] Jeffrey M. Bielicki[agh]

Table of Contents

1 Supplemental Figures **2**

2 Supplemental Tables **20**

3 Estimating the Water Withdrawal Intensities of Coal-Fired Power Plants **24**

3.1 Cooling Water Withdrawal Intensities 24

3.1.1 Thermal Efficiency under Wet and Dry Cooling (η_{net}) and Flue Gas Loss (k_{os}) 25

3.1.2 Parameters Related to the Cooling Systems 28

3.2 Non-Cooling Water Use at the Coal-Fired Power Plants 29

4 Sensitivity Analysis and Validation of the Modeled Water Withdrawal Intensities **31**

5 Sensitivity of the Usable Capacity (*UC*) and Usable Capacity Factor (*UF*) to Environmental Flow Methods and Minimum Load Levels **34**

---

[a] Environmental Science Graduate Program, The Ohio State University, USA

[b] International Institute for Applied Systems Analysis, Laxenburg, Austria

[c] Current affiliation: Institute for a Secure and Sustainable Environment, University of Tennessee, USA. Email: ywang254@utk.edu

[d] Institute for Integrated Energy Systems, University of Victoria, Victoria, Canada

[e] Department of Physical Geography, Utrecht University, The Netherlands

[f] Environmental Sciences Division and Climate Change Science Institute, Oak Ridge National Laboratory, USA

[g] Department of Civil, Environmental, and Geodetic Engineering, The Ohio State University, USA

[h] John Glenn College of Public Affairs, The Ohio State University, USA

6 Scenarios of Coal-Fired Power Plants Construction and Retirement under Carbon Emission Mitigation....39

6.1 ASIA Regional Scenarios 39

6.2 National Total Installed Coal Capacity 42

6.3 Local Installed Coal Capacity 48

6.4 Local Scenarios of CO_2 Capture and Storage (CCS) Deployment 50

7 The Energy Penalty of Dry Cooling Relative to Cooling Towers 54

1 Supplemental Figures

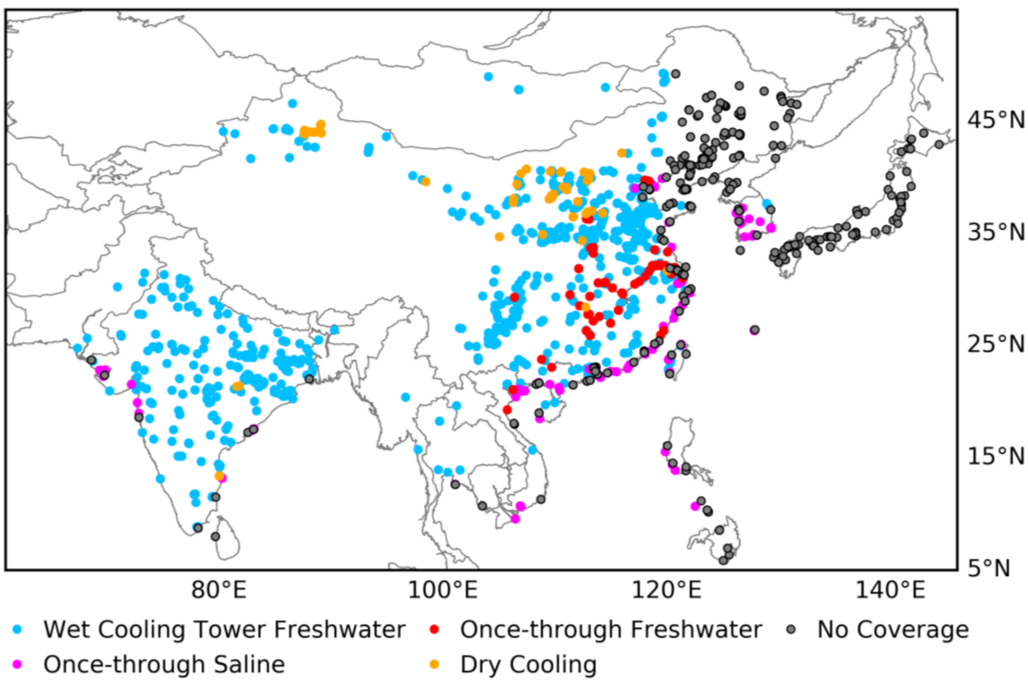

Figure S1. The Existing Coal-Fired Power Plants in the GCPT17 dataset[1] That are in and Outside the Coverage of the PCR-GLOBWB 2 Simulations. Colors show cooling system choices that are from a geo-referenced coal-fired power plants dataset[2,3].

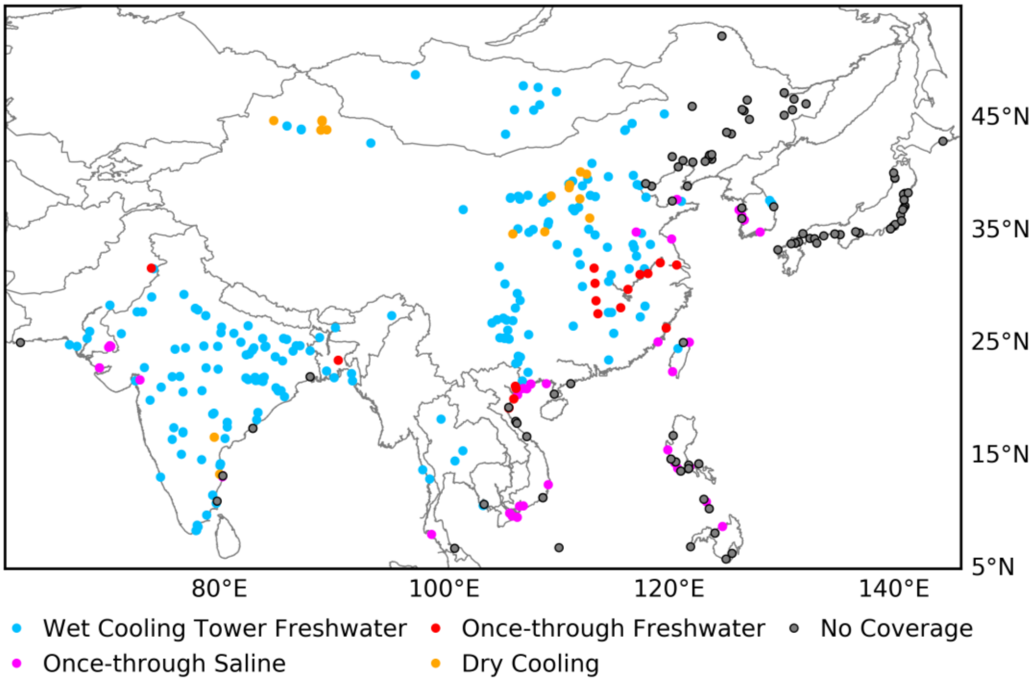

Figure S2. The Planned Coal-Fired Power Plants in the GCPT17 dataset[1] That are in and Outside the Coverage of the PCR-GLOBWB 2 Simulations. Colors show cooling system choices under the Business-as-Usual case, i.e. each planned power plant use the same type of cooling system as the nearest existing plant unless otherwise required by regulation.

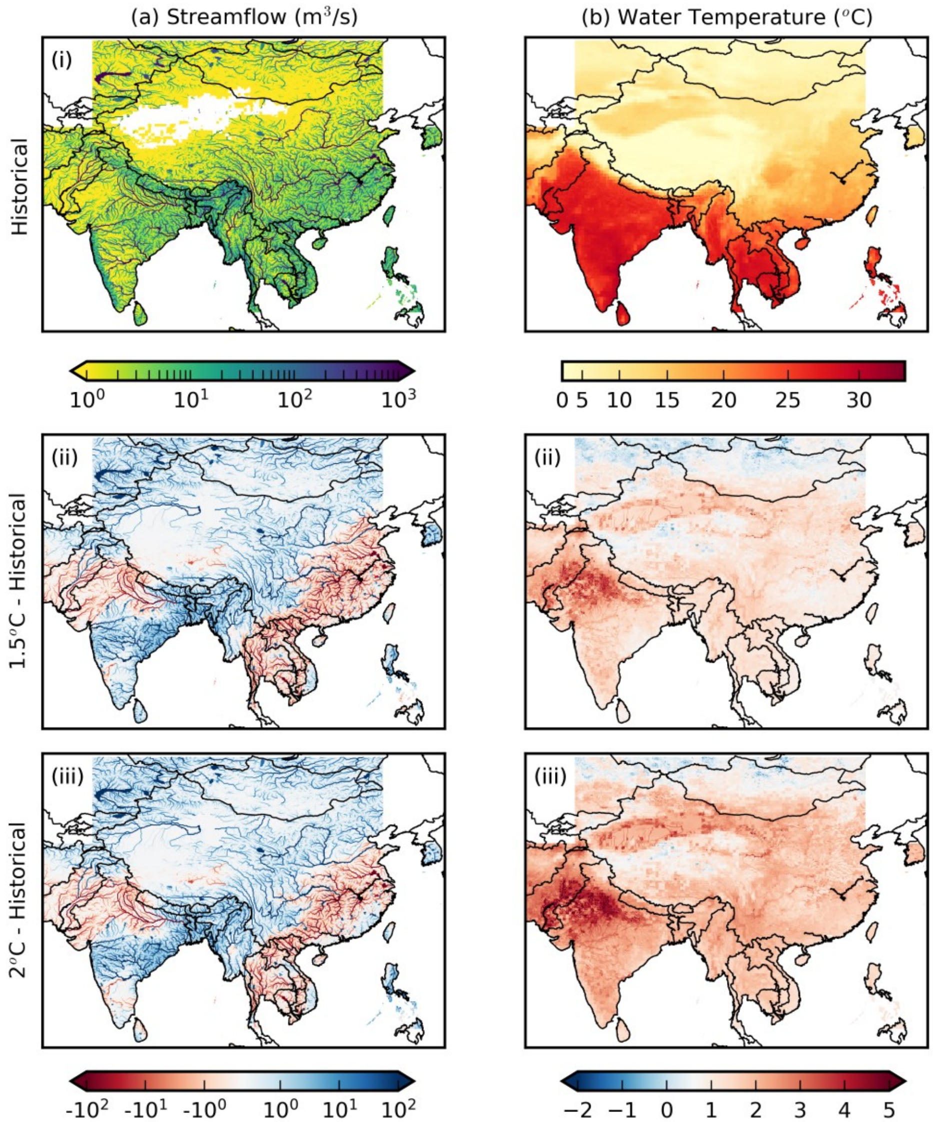

Figure S3. Estimated (a) Annual Mean Streamflow, and (b) Annual Mean Water Temperature. Results are from PCR-GLOBWB 2 simulations using downscaled meteorological inputs from the GFDL-ESM2M global climate model. (i) Historical baseline (1961-1990), and the differences between the (ii) 1.5ºC, and (iii) 2ºC scenarios of climate change and the historical baseline.

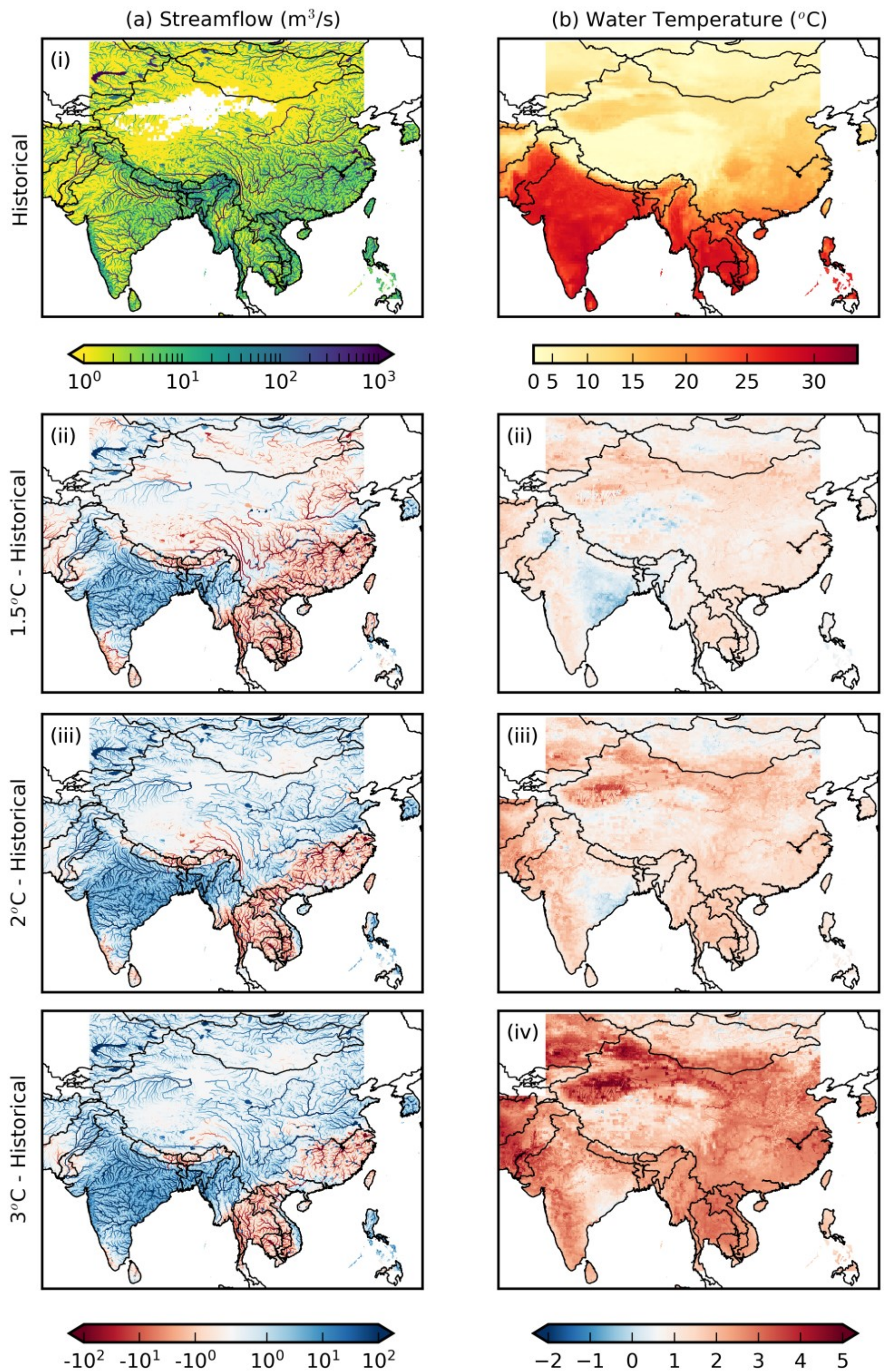

Figure S4. Estimated (a) Annual Mean Streamflow, and (b) Annual Mean Water Temperature. Results are from PCR-GLOBWB 2 simulations using downscaled meteorological inputs from the HadGEM2-ES global climate model. (i) Historical baseline (1961-1990), and the differences between the (ii) 1.5ºC, (iii) 2ºC, and (iv) 3ºC scenarios of climate change and the historical baseline.

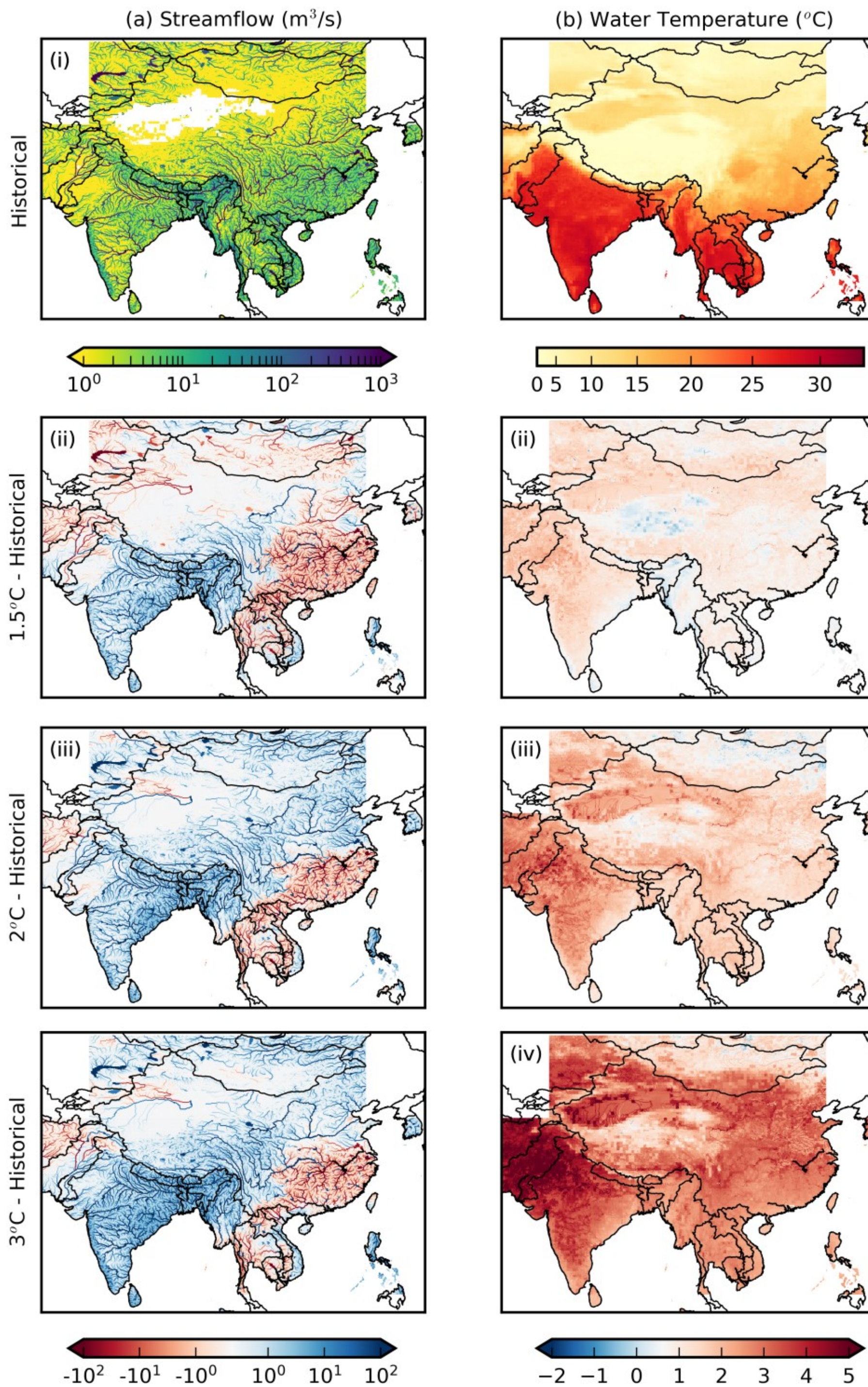

Figure S5. Estimated (a) Annual Mean Streamflow, and (b) Annual Mean Water Temperature. Results are from PCR-GLOBWB 2 simulations using downscaled meteorological inputs from the IPSL-CM5A-LR global climate model. (i) Historical baseline (1961-1990), and the differences between the (ii) 1.5°C, (iii) 2°C, and (iv) 3°C scenarios of climate change and the historical baseline.

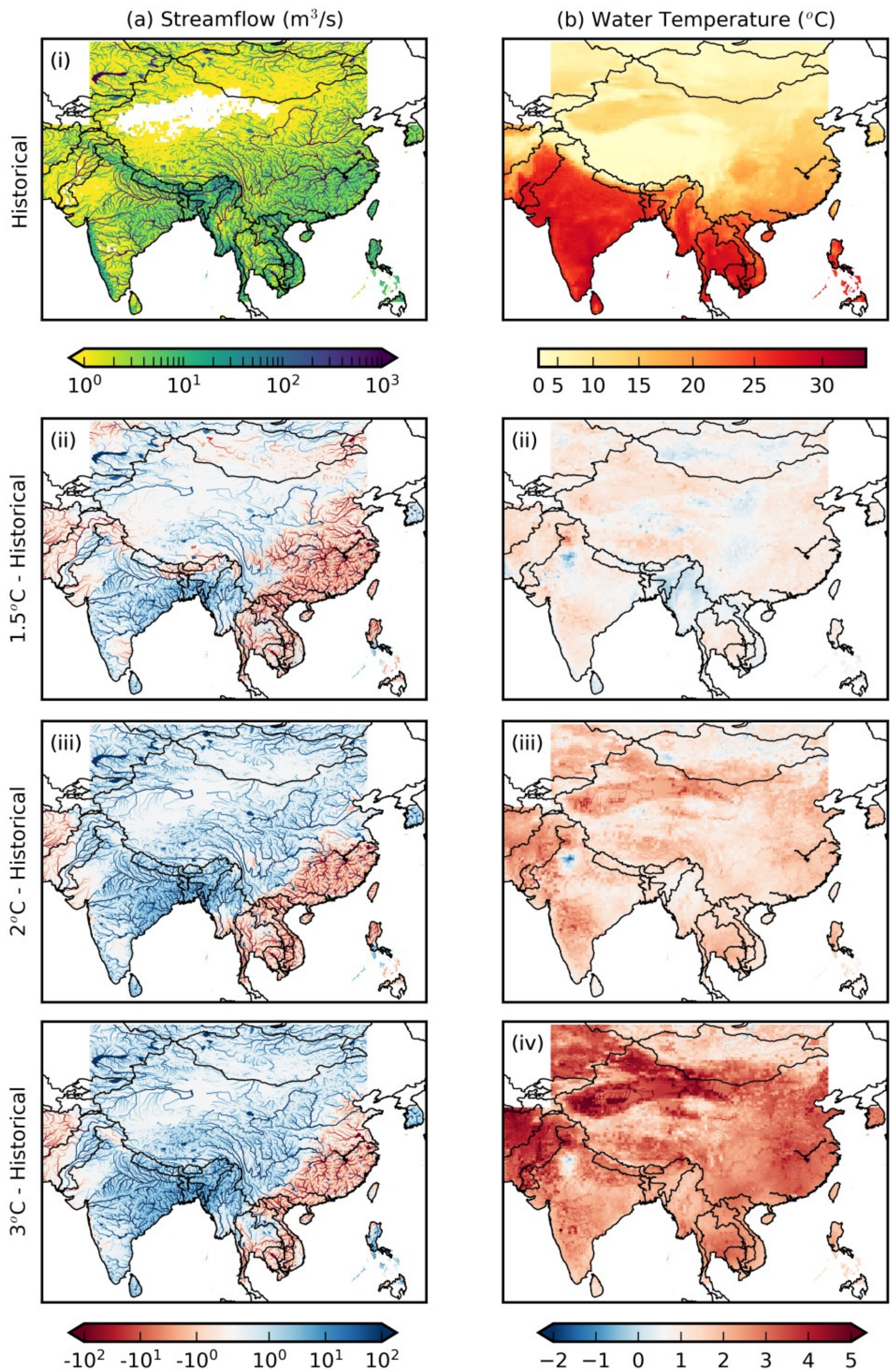

Figure S6. Estimated (a) Annual Mean Streamflow, and (b) Annual Mean Water Temperature. Results are from PCR-GLOBWB 2 simulations using downscaled meteorological inputs from the MIROC-ESM-CHEM global climate model. (i) Historical baseline (1961-1990), and the differences between the (ii) 1.5ºC, (iii) 2ºC, and (iv) 3ºC scenarios of climate change and the historical baseline.

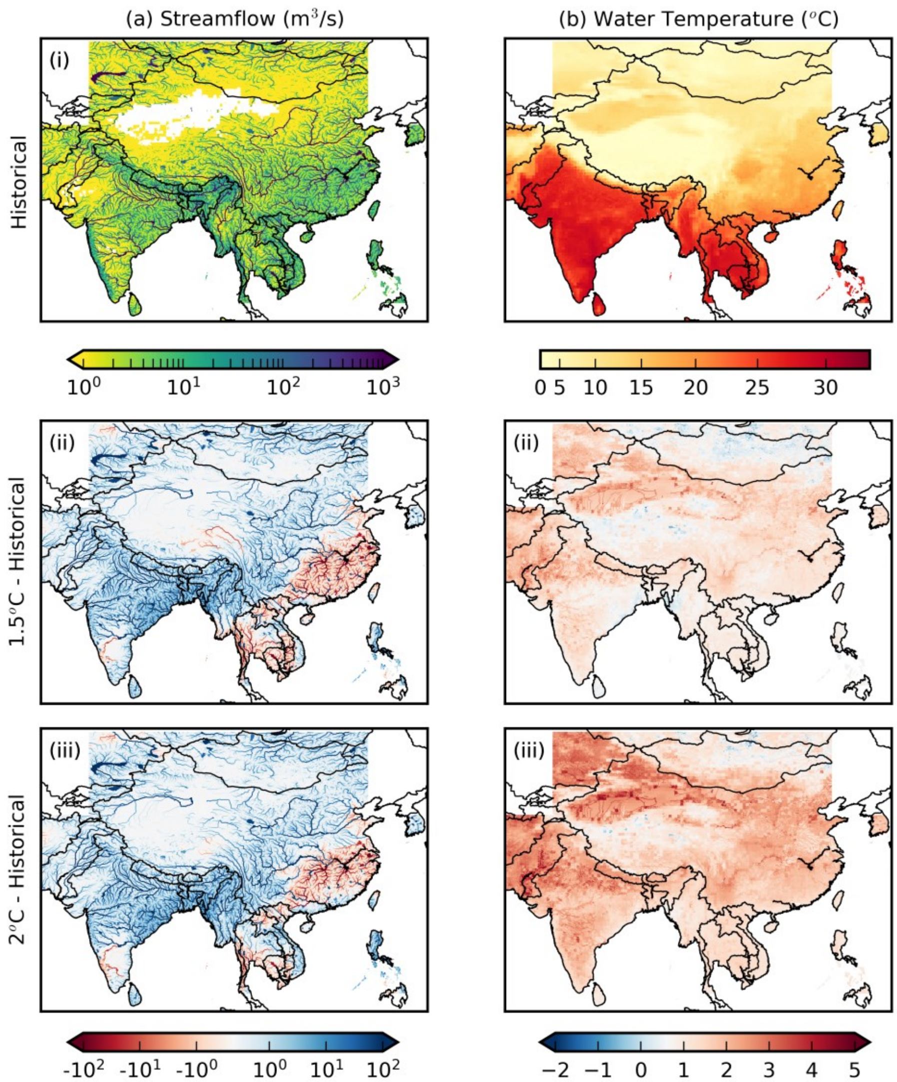

Figure S7. Estimated (a) Annual Mean Streamflow, and (b) Annual Mean Water Temperature. Results are from PCR-GLOBWB 2 simulations using downscaled meteorological inputs from the NorESM1-M global climate model. (i) Historical baseline (1961-1990), and the differences between the (ii) 1.5ºC, (iii) 2ºC, and (iv) 3ºC scenarios of climate change and the historical baseline.

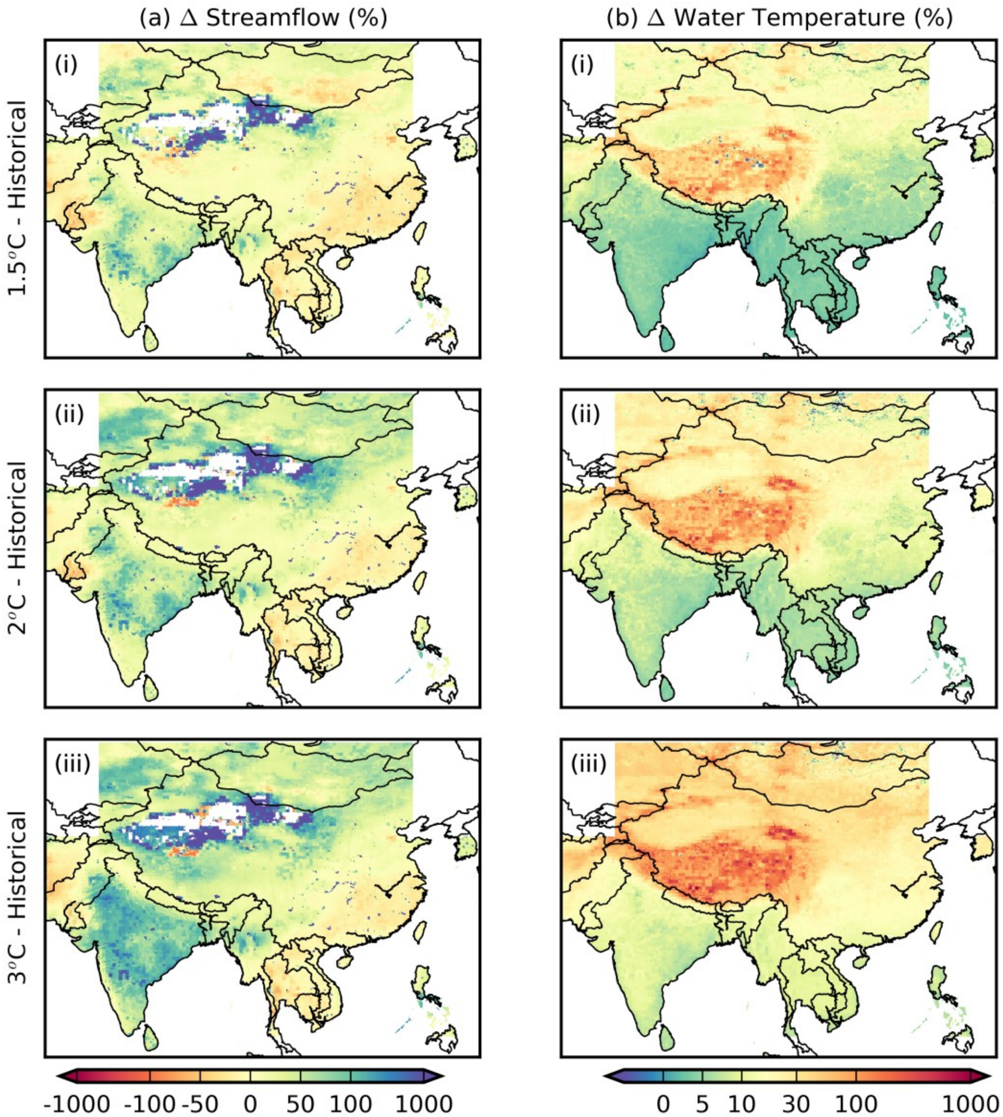

Figure S8. Estimated Percentage Changes in (a) Annual Mean Streamflow, and (b) Annual Mean Water Temperature between the Historical Baseline (1961-1990) and (i) 1.5°C, (ii) 2°C, and (iii) 3°C Scenarios of Climate Change. Results are from PCR-GLOBWB 2 simulations, averaged over the global climate models. The percentage changes are defined by the difference between future streamflow (water temperature) and historical streamflow (water temperature), divided by the historical streamflow (water temperature), and multiplied by 100%.

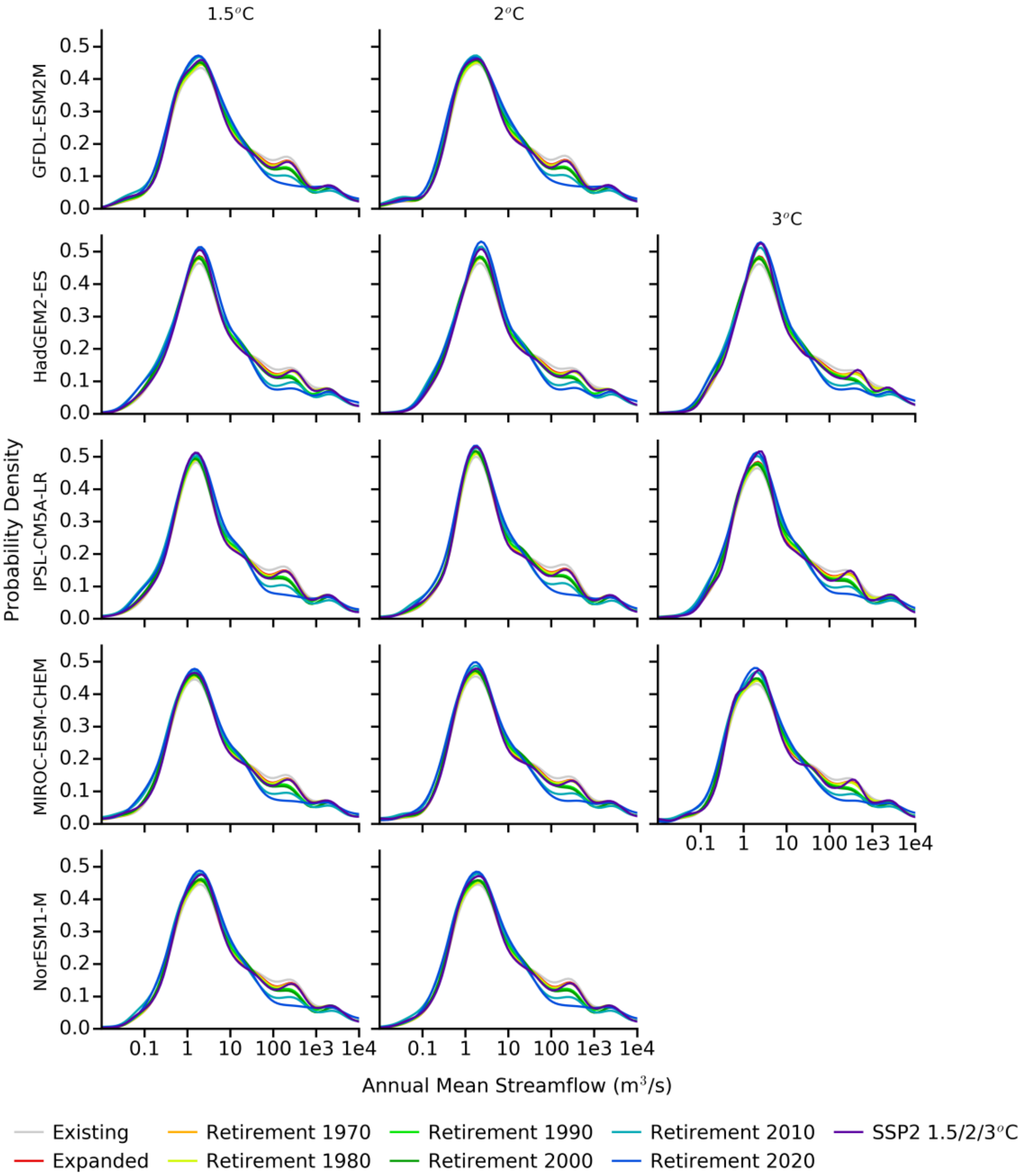

Figure S9. Nameplate Capacity-Weighted Probability Density Distributions of the Annual Mean Streamflow at the Grid Cells Occupied by Coal-Fired Power Plants for All Scenarios of Climate Change, Global Climate Models, and Cases of Capacity Expansion. The probability density distributions were smoothed by kernel density estimation for better readability. The weighting by nameplate capacity is in the sense the number of "observations" that each grid cell contributes to the probability density distribution is proportional to the total nameplate capacity installed in the grid cell.

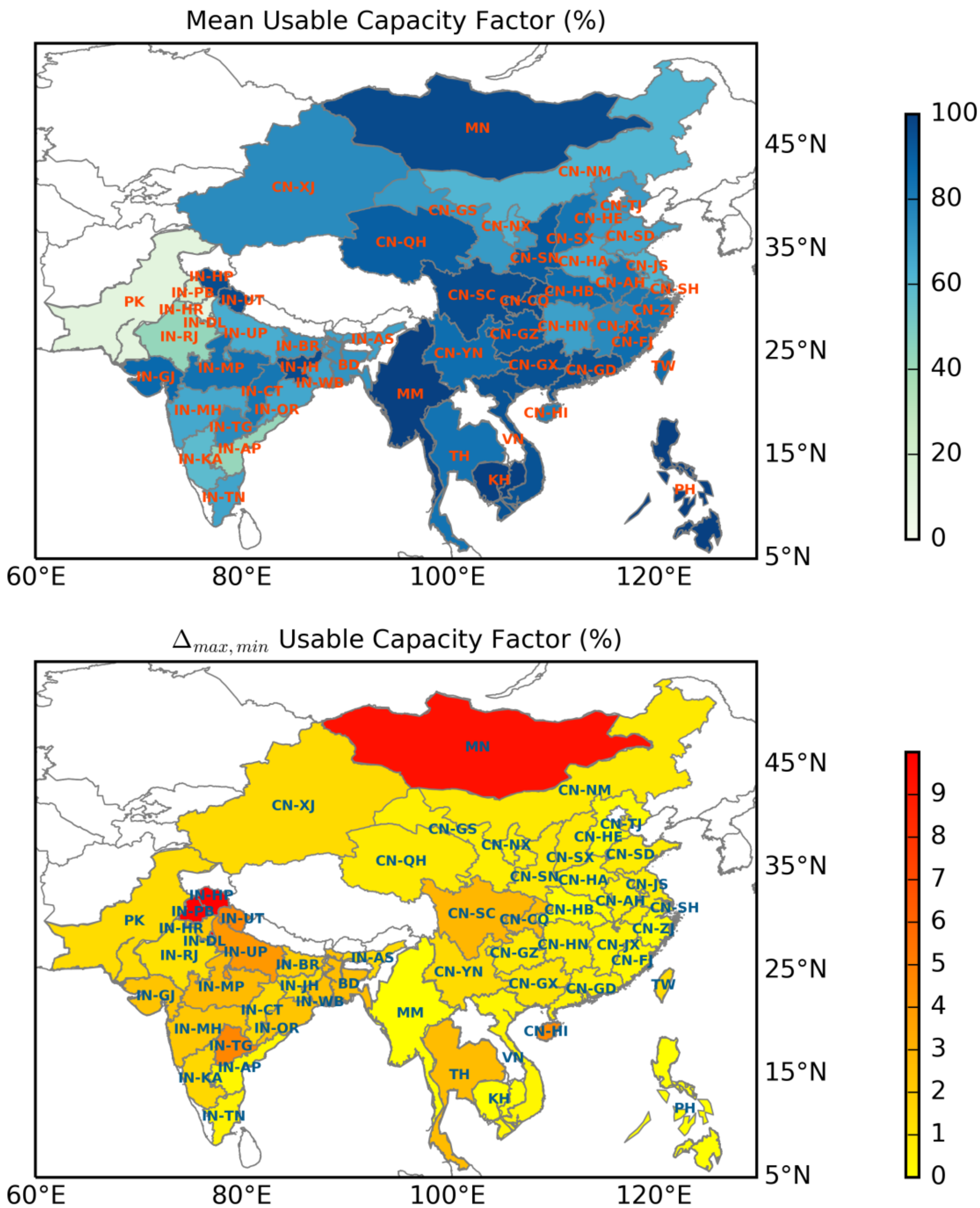

Figure S10. The Mean Annual Average Usable Capacity Factors during the Historical Baseline (1961-1990) (Top) and the Range across the GCMs (Bottom) at Administrative Unit-Level. The country, country-province (China), country-state (India) abbreviations follow the ISO 3166-1:2013 and ISO 3166-2:2013 standards.[4,5]

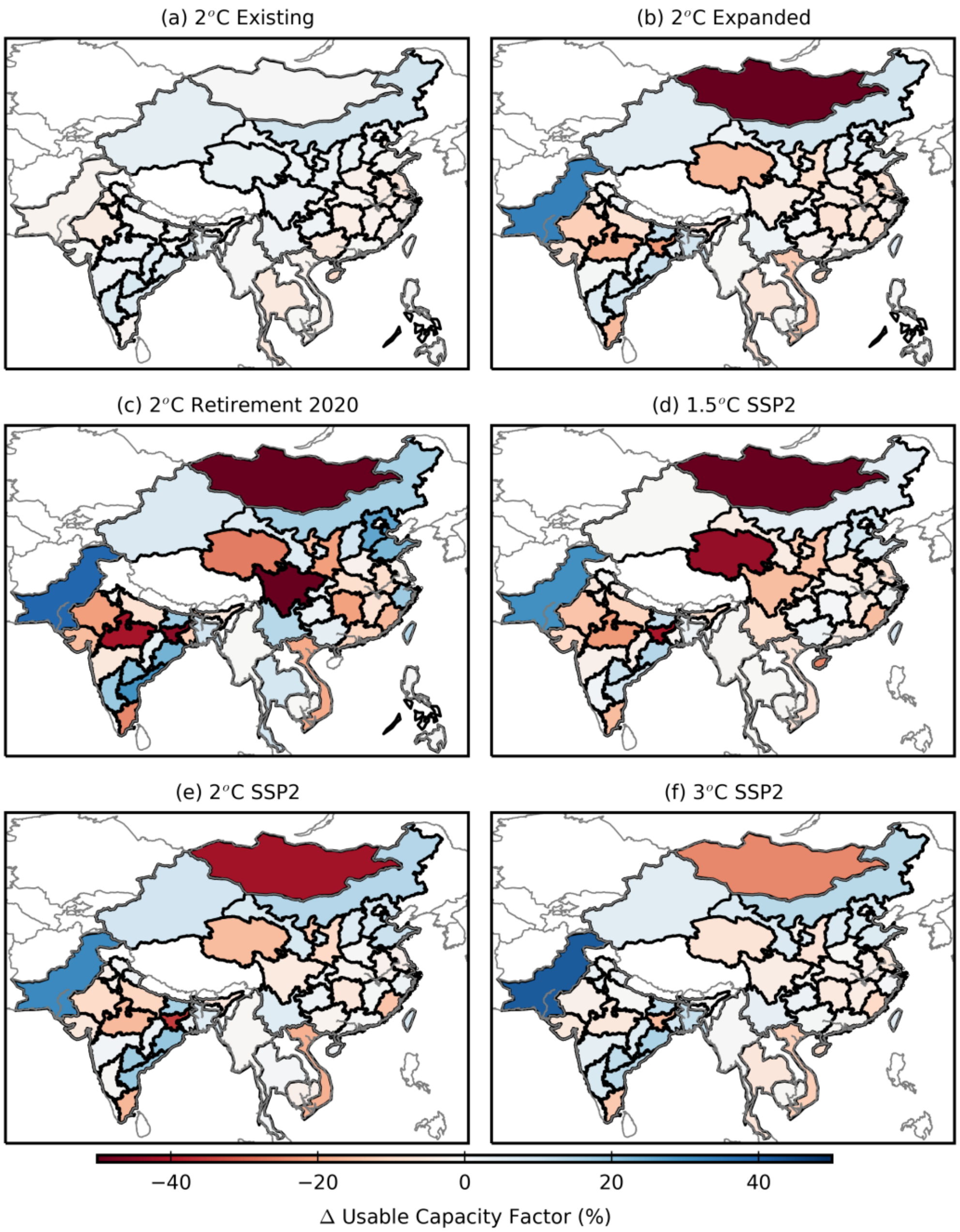

Figure S11. Minimum Changes in Annual Average Usable Capacity Factors (*UF*) from the Historical Baseline (1961-1990, the *Existing* case) to Selected Future Climate Scenarios and Cases of Capacity Expansion. "Minimum": the values displayed in the maps are based on the minimum of the state-level (India), province-level (China), or country-level (the other Asian countries) *UF*'s across the GCMs.

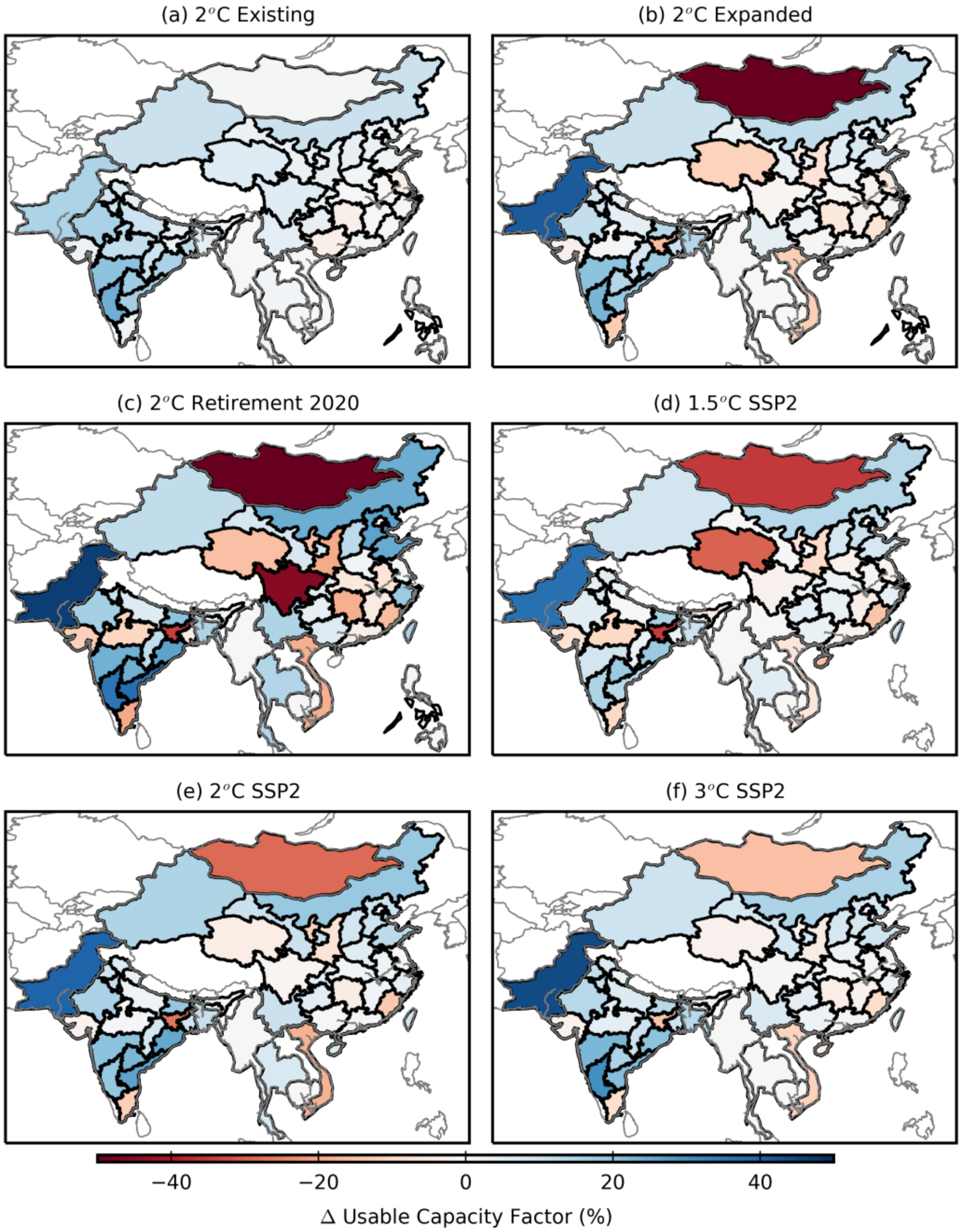

Figure S12. Maximum Changes in Annual Average Usable Capacity Factors (*UF*) from the Historical Baseline (1961-1990, the *Existing* case) to Selected Future Climate Scenarios and Cases of Capacity Expansion. "Maximum": the values displayed in the maps are based on the maximum of the state-level (India), province-level (China), or country-level (the other Asian countries) *UF*'s across the GCMs.

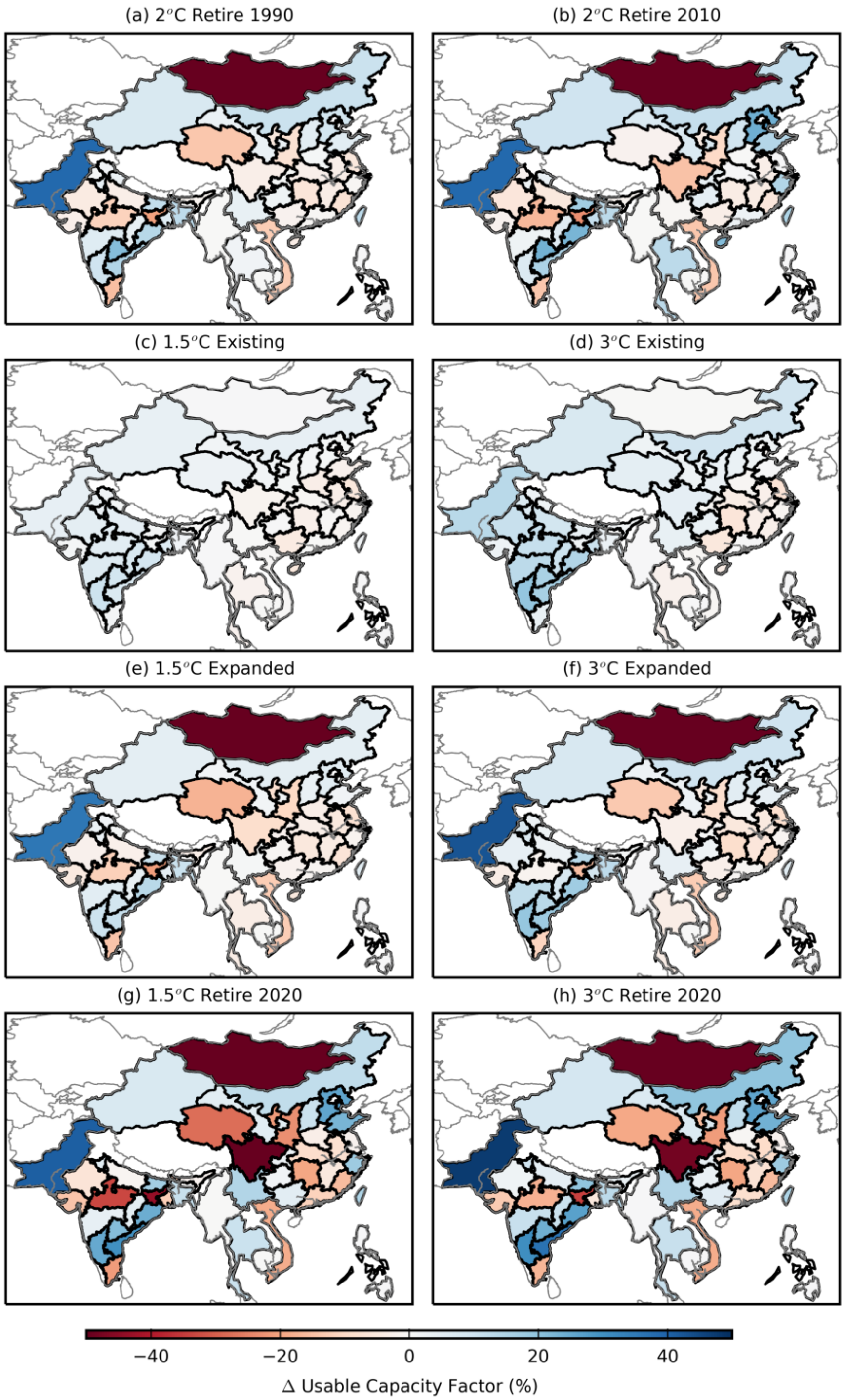

Figure S13. Average Changes in Annual Average Usable Capacity Factors (*UF*) from the Historical Baseline (1961-1990, the *Existing* case) to Selected Future Climate Scenarios and Cases of Capacity Expansion. "Average": the values displayed in the maps are based on the average of the state-level (India), province-level (China), or country-level (the other Asian countries) *UF*'s across the GCMs.

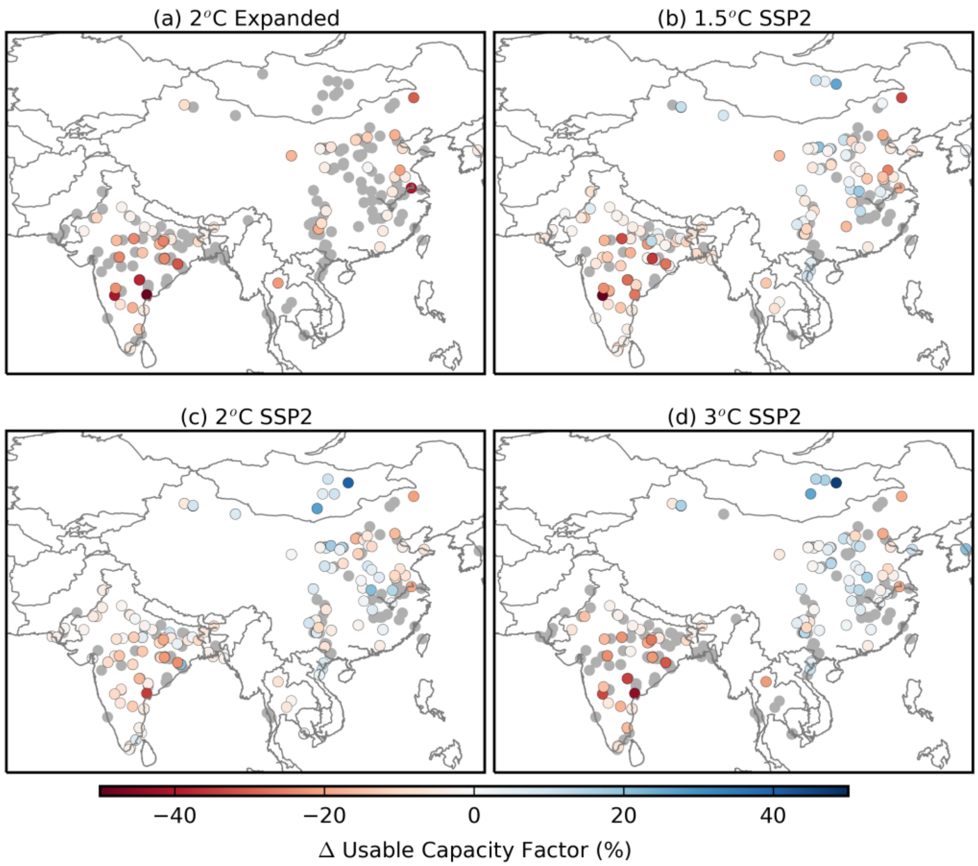

Figure S14. Changes in the Usable Capacity Factors of Individual Coal-Fired Power Plants That are in the Planned Fleet between the Historical Baseline (1961-1990, the *Existing Capacity* Case) and Selected Future Climate Scenarios and Cases of Capacity Expansion. Gray dots indicate where the changes are within ±1% of the nameplate capacity. The values are averages across the GCMs.

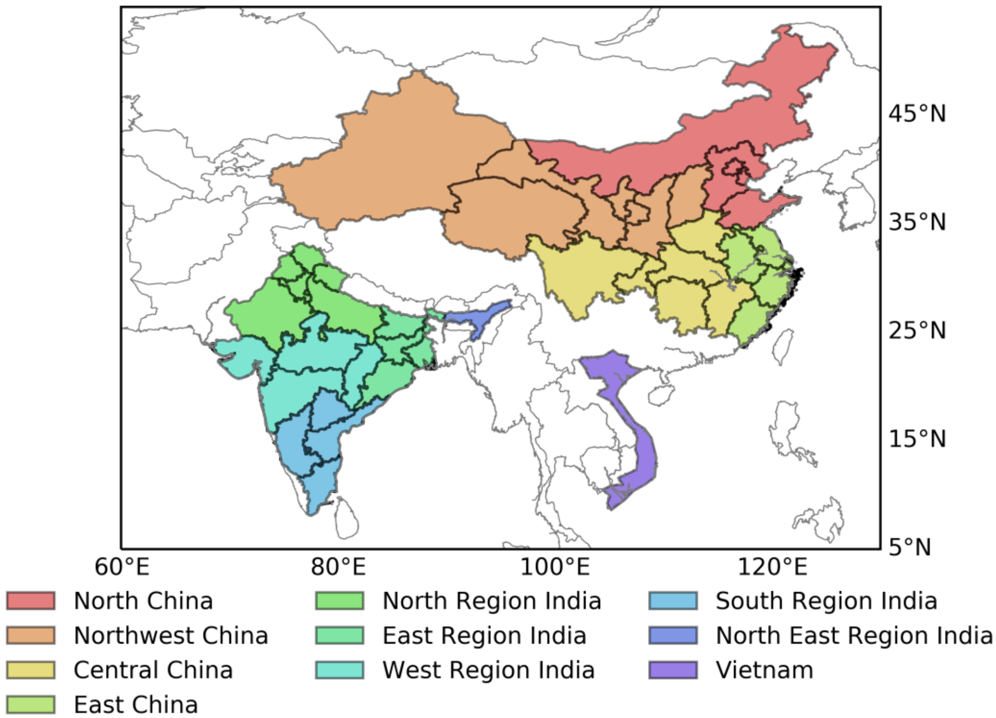

Figure S15. The Spatial Extents of Regional Power Grids Used in This Study.

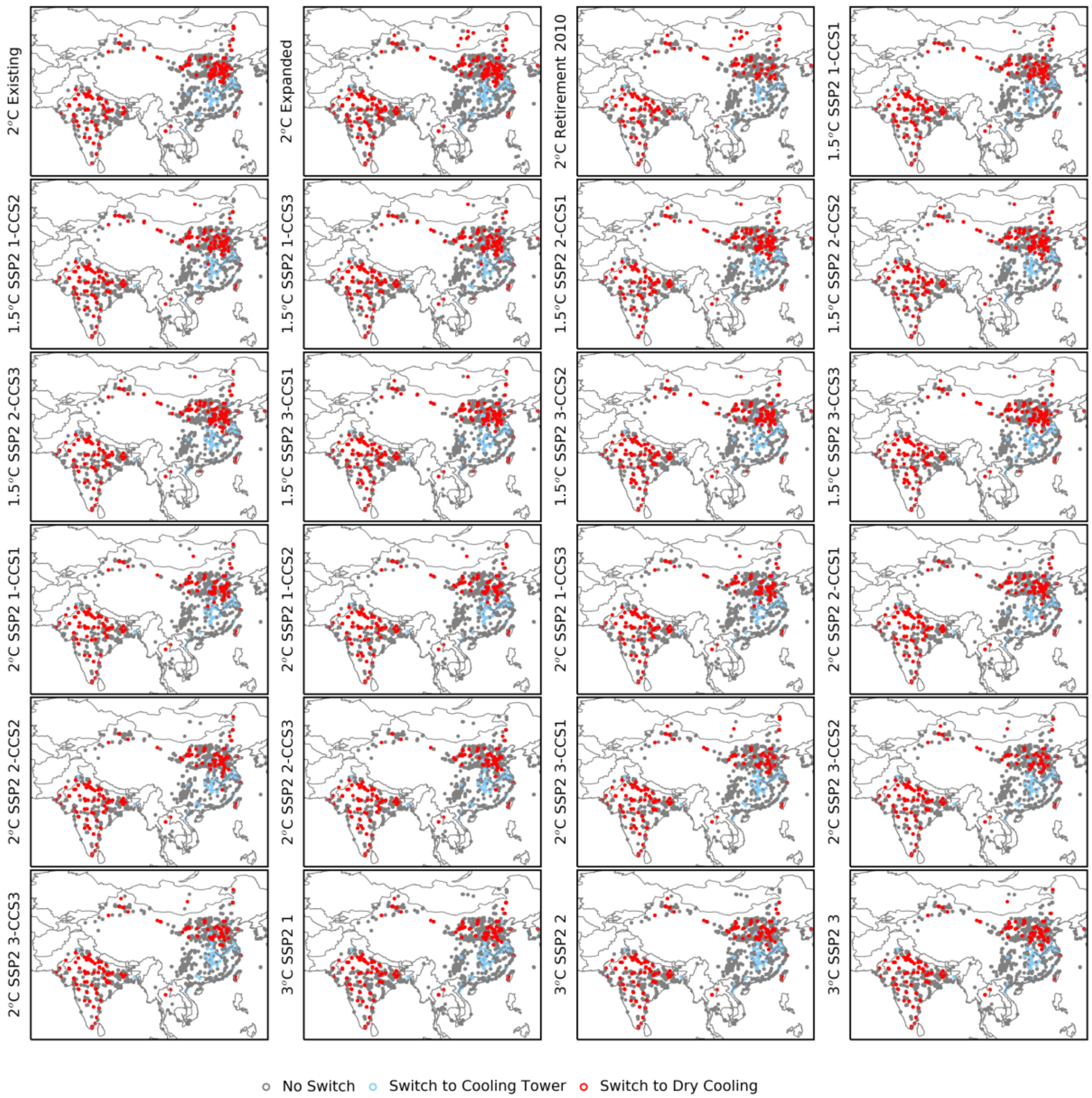

Figure S16. Location of the Coal-Fired Power Plants that Switched from Once-Through to Cooling Tower, or from Cooling Tower to Dry Cooling Systems for Selected Climate Change and Capacity Expansion Scenarios. The different random samples are shown for the *Regional Transformation* scenarios.

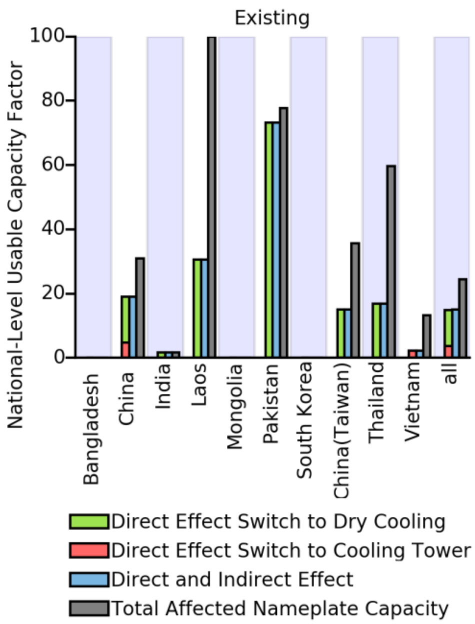

Figure S17. Direct and Indirect Effects of Switching to Wet Cooling Tower and Dry Cooling Systems on the National-Level *UF*'s under Historical Conditions and Various Cases of Capacity Expansion. The banded background distinguishes between different countries.

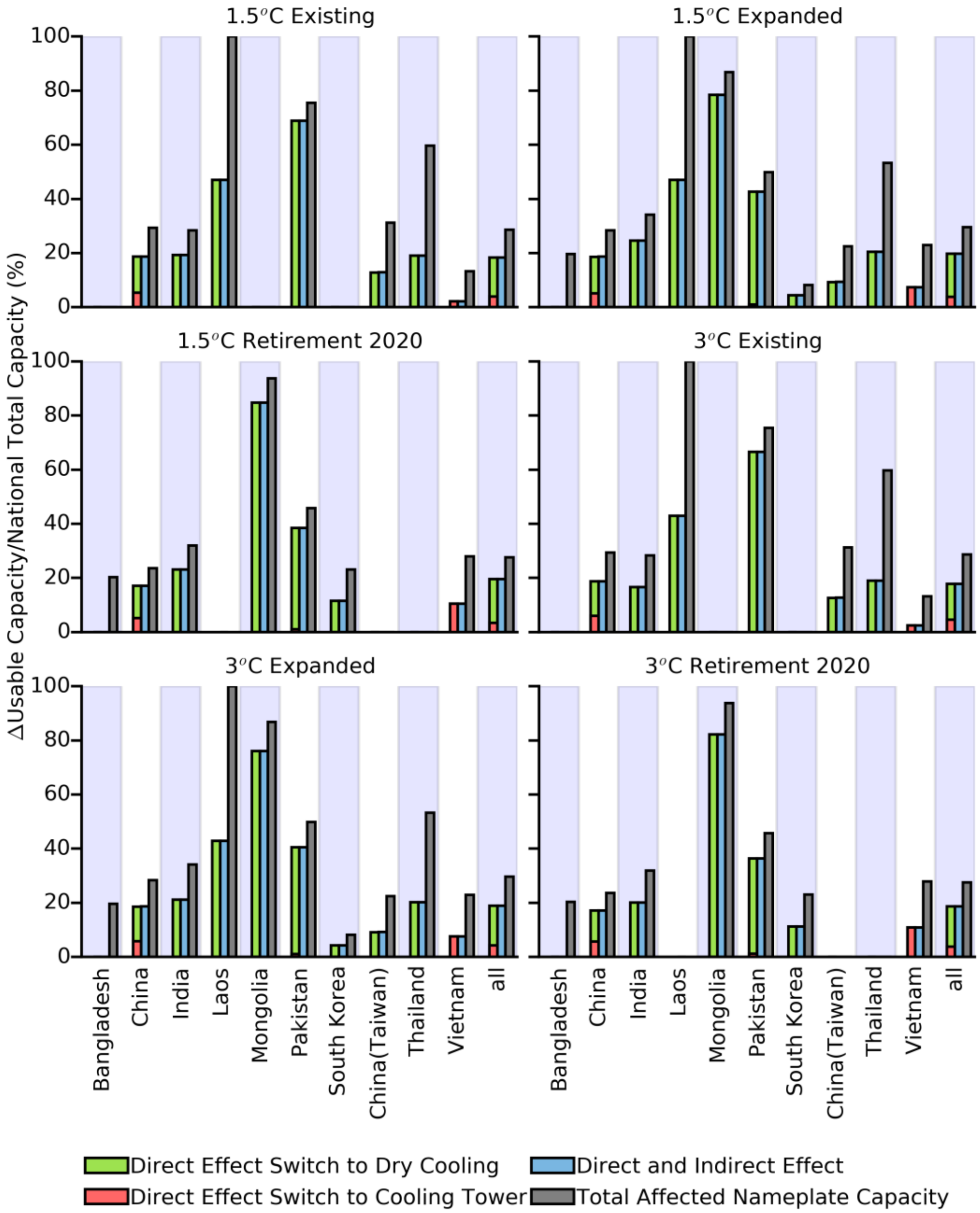

Figure S18. Direct and Indirect Effects of Switching to Wet Cooling Tower and Dry Cooling Systems on the National-Level *UC*'s under Various Cases of Capacity Expansion. The banded background distinguishes between different countries.

2 Supplemental Tables

Table S1. The Total Nameplate Capacity of Installed Coal-Fired Power Plants (MW) for All the Scenarios of Capacity Expansion for the Whole Region, and by Country, (for India) State, or (for China) Province. The percentages of nameplate capacity fitted with CO_2 capture and storage (CCS) are shown for the two SSP2-downscaled scenarios of capacity expansion (AIM/CGE SSP2-26, corresponding to ~1.5°C global warming, and AIM/CGE SSP2-34, corresponding to ~2°C global warming) that use CCS. The variability between random samples for each SSP2-downscaled scenario are shown as the deviations of the minimum and the maximum from the sample-mean.

Scenario	Exist	Expanded	Retirement 1970	1980	1990	2000	2010	2020	AIM/CGE SSP2-26 (1.5 °C) Installed Capacity (MW) Mean	(-/+)	CCS (%) Mean	(-%/+%)	AIM/CGE SSP2-34 (2°C) Installed Capacity (MW) Mean	(-/+)	CCS (%) Mean	(-%/+%)	MESSAGE-GLOBIOM SSP2-60 (3°C) Installed Capacity (MW) Mean	(-/+)
			Installed Capacity (MW)															
Whole Region	1,040,767	1,454,178	1,447,181	1,437,276	1,386,476	1,281,321	899,450	413,411	622,600	(0,42)	76.6%	(-0.4,1.0)	640,097	(-102,91)	54.3%	(0.0,0.1)	1,004,909	(-5,6)
Bangladesh	250	7,070	7,070	7,070	7,070	7,070	6,820	6,820	7,070	(0,0)	81.9%	(-18.4,18.1)	7,070	(0,0)	52.8%	(-17.8,20.4)	0	(0,0)
Cambodia	270	1,310	1,310	1,310	1,310	1,310	1,310	1,040	905	(0,0)	87.7%	(-43.0,12.3)	1,040	(0,0)	70.4%	(-31.5,29.6)	0	(0,0)
Japan	780	780	624	624	312	0	0	0	624	(0,0)	91.7%	(-16.7,8.3)	624	(0,0)	44.4%	(-19.4,30.6)	0	(0,0)
Laos	1,878	1,878	1,878	1,878	1,878	1,878	1,878	0	626	(0,0)	88.9%	(-88.9,11.1)	626	(0,0)	11.1%	(-11.1,88.9)	0	(0,0)
Mongolia	706	9,486	9,486	9,486	8,880	8,880	8,880	8,780	500	(0,0)	84.4%	(-54.4,15.6)	525	(-9,5)	90.4%	(-48.5,9.6)	0	(0,0)
Myanmar	160	710	710	710	710	710	590	550	710	(0,0)	100.0%	(0.0,0.0)	710	(0,0)	76.5%	(-46.9,23.5)	0	(0,0)
Pakistan	1,750	12,695	12,695	12,695	12,695	12,545	12,545	10,945	12,695	(0,0)	72.0%	(-24.0,12.4)	12,695	(0,0)	50.7%	(-15.4,18.2)	0	(0,0)
Philippines	2,976	7,197	7,197	7,197	6,897	5,937	5,705	4,221	0	(0,0)	0.0%	(0.0,0.0)	0	(0,0)	0.0%	(0.0,0.0)	0	(0,0)
South Korea	18,774	27,778	27,778	26,289	25,289	18,397	13,311	9,004	8,500	(0,0)	76.3%	(-19.2,11.9)	8,595	(-3,2)	52.3%	(-14.4,13.4)	0	(0,0)
Taiwan	8,355	11,604	11,604	11,604	9,377	7,277	3,249	3,249	8,630	(-1,2)	71.1%	(-14.0,15.6)	8,706	(-4,4)	54.2%	(-11.6,13.7)	0	(0,0)
Thailand	4,023	5,629	5,629	5,629	5,029	2,387	2,351	1,606	2,305	(-3,2)	84.9%	(-32.6,15.1)	2,476	(0,1)	56.7%	(-25.4,25.1)	0	(0,0)
Vietnam	12,377	36,202	36,202	36,097	35,657	35,657	33,873	23,825	7,497	(-2,2)	75.2%	(-9.5,8.5)	8,071	(-2,4)	65.9%	(-18.4,19.3)	0	(0,0)
China Anhui	46,355	56,945	56,945	56,945	55,675	52,590	31,805	10,590	22,348	(-8,7)	77.2%	(-14.5,12.7)	22,740	(-10,5)	54.0%	(-11.3,12.5)	34,063	(-3,2)
Chongqing	12,965	15,490	15,490	15,490	15,490	13,950	10,135	2,525	6,078	(-3,2)	80.0%	(-12.2,20.0)	6,183	(-3,7)	57.4%	(-30.7,32.0)	9,265	(0,0)
Fujian	17,236	28,016	28,016	28,016	27,316	25,906	16,800	10,780	10,994	(-9,9)	66.3%	(-22.0,24.2)	11,186	(-3,2)	44.5%	(-21.9,15.7)	16,757	(-9,8)
Gansu	18,710	25,110	25,110	25,110	24,780	23,040	14,300	6,400	9,850	(-5,5)	79.0%	(-33.1,14.6)	10,022	(-2,3)	47.5%	(-13.8,10.9)	15,018	(-3,2)
Guangdong	35,567	37,667	37,487	37,487	37,127	32,672	20,865	2,100	14,782	(-7,7)	74.6%	(-19.2,12.4)	15,042	(-3,2)	50.7%	(-17.0,10.1)	22,529	(-3,7)
Guangxi	12,845	17,064	16,964	16,764	16,764	16,294	10,779	4,219	6,692	(-3,7)	86.2%	(-30.6,8.4)	6,813	(-3,2)	60.1%	(-19.7,23.1)	10,207	(-3,2)
Guizhou	28,700	51,280	51,280	51,280	51,280	50,680	35,880	22,580	20,120	(0,0)	78.7%	(-22.4,16.6)	20,477	(-7,3)	52.4%	(-13.7,13.2)	30,667	(-7,3)
Hainan	2,074	2,074	2,074	2,074	2,074	1,660	700	0	810	(0,0)	63.8%	(-45.3,36.2)	830	(0,0)	51.1%	(-51.1,30.8)	1,244	(0,0)
Hebei	36,916	46,516	46,416	45,816	44,596	37,536	19,810	9,600	18,249	(-3,4)	76.4%	(-5.0,9.2)	18,572	(-9,8)	50.8%	(-12.7,8.0)	27,824	(-4,4)
Henan	60,660	68,700	67,780	67,480	66,140	61,140	31,680	8,040	26,958	(-3,2)	72.7%	(-9.2,8.2)	27,435	(0,0)	53.5%	(-8.9,12.8)	41,097	(-7,3)
Hong Kong	6,608	6,608	6,608	6,608	1,727	0	0	0	2,585	(-8,15)	70.1%	(-37.1,29.9)	2,631	(0,0)	42.2%	(-32.7,44.5)	3,954	(0,0)
Hubei	22,740	33,420	33,420	33,420	33,300	28,200	19,110	10,680	13,110	(0,0)	73.9%	(-6.2,10.8)	13,347	(-17,13)	61.8%	(-9.3,18.8)	19,990	(0,0)
Hunan	19,564	23,624	23,624	23,624	23,204	21,280	9,160	4,060	9,279	(-7,6)	74.2%	(-12.8,19.3)	9,430	(-10,12)	54.0%	(-19.1,18.9)	14,133	(-9,6)
Inner Mongolia	74,462	90,772	89,960	89,960	89,260	85,440	49,330	16,310	35,612	(-7,10)	74.5%	(-10.8,9.3)	36,254	(-2,1)	53.6%	(-10.0,13.2)	54,272	(-15,20)
Jiangsu	59,093	67,113	66,902	66,572	64,170	57,714	30,590	8,020	26,325	(-8,8)	77.8%	(-4.1,5.9)	26,789	(-6,5)	52.8%	(-5.7,8.4)	40,148	(-15,7)
Jiangxi	17,230	29,974	29,974	29,974	29,974	28,514	20,164	12,744	11,756	(-4,6)	67.4%	(-16.0,12.4)	11,977	(-7,5)	51.0%	(-17.1,18.4)	17,932	(0,0)
Ningxia	20,350	32,510	32,300	32,250	32,200	30,780	23,970	12,160	12,757	(-2,3)	71.8%	(-15.2,23.0)	12,977	(-7,13)	47.7%	(-9.5,12.0)	19,448	(-8,7)
Qinghai	3,160	4,480	4,480	4,480	4,480	4,480	3,340	1,320	1,755	(0,0)	77.6%	(-69.9,22.4)	1,795	(0,0)	60.9%	(-44.2,39.1)	2,677	(-2,3)
Shaanxi	30,030	51,010	50,810	50,810	50,810	48,080	32,200	20,980	20,020	(-10,5)	75.9%	(-11.4,6.4)	20,363	(-8,12)	53.8%	(-14.7,9.4)	30,510	(-5,5)
Shandong	76,149	93,849	93,519	93,519	90,674	83,945	53,038	17,700	36,831	(-10,6)	76.2%	(-6.1,6.1)	37,476	(-13,11)	55.6%	(-7.0,7.6)	56,136	(-17,17)
Shanghai	8,020	8,020	7,770	7,670	6,695	5,120	2,000	0	3,148	(-3,2)	73.5%	(-37.0,26.5)	3,200	(0,0)	35.4%	(-32.3,33.3)	4,795	(0,0)
Shanxi	56,683	75,063	74,877	74,877	73,467	69,727	41,542	18,380	29,458	(-2,4)	80.1%	(-7.6,7.1)	29,968	(-7,9)	58.6%	(-7.1,15.0)	44,902	(-5,5)
Sichuan	12,415	14,415	14,415	14,415	14,215	12,935	5,495	2,000	5,655	(0,0)	79.0%	(-23.2,10.4)	5,753	(-3,2)	52.8%	(-17.6,15.4)	8,622	(-2,3)
Tianjin	8,372	9,522	9,522	9,522	9,082	6,066	2,950	1,150	3,737	(-1,1)	81.8%	(-16.1,18.2)	3,801	(-1,3)	66.1%	(-18.9,24.7)	5,696	(0,0)
Xinjiang	46,440	70,870	70,475	70,475	70,475	69,695	64,230	24,430	27,808	(-18,17)	75.4%	(-8.2,6.7)	28,298	(-3,7)	54.7%	(-7.4,13.2)	42,390	(-5,5)

	Yunnan	12,835	13,435	13,435	13,435	13,435	12,435	4,200	600	5,285	(0,0)	75.0%(-24.2,21.2)	5,362	(-12,23)	61.1%(-16.8,12.8)	8,035	(0,0)
	Zhejiang	30,807	30,957	30,920	30,920	30,275	27,388	11,385	150	12,150	(-10,5)	68.5%(-14.6,12.8)	12,362	(-3,4)	45.4%(-15.4,24.0)	18,516	(-3,4)
India	**Andhra Pradesh**	10,551	16,751	16,688	16,478	15,938	14,761	12,774	6,200	9,129	(-7,5)	74.1%(-15.5,13.2)	9,619	(-8,4)	55.8%(-27.2,16.3)	16,751	(0,0)
	Assam	500	1,410	1,410	1,410	1,410	1,410	1,410	910	750	(0,0)	100.0% (0.0,0.0)	750	(0,0)	63.0%(-29.6,37.0)	1,410	(0,0)
	Bihar	5,650	15,270	15,270	15,270	14,830	13,990	12,990	9,620	8,320	(0,0)	83.8%(-39.8,16.2)	8,765	(-5,5)	31.2% (-9.9,9.9)	15,270	(0,0)
	Chhattisgarh	23,791	33,811	33,364	33,244	29,856	29,856	25,541	10,020	18,420	(-5,5)	79.5% (-15.8,8.5)	19,408	(-4,6)	63.4%(-13.2,17.2)	33,811	(0,0)
	Delhi	705	705	705	210	0	0	0	0	400	(0,0)	88.3%(-40.8,11.7)	400	(0,0)	70.8%(-23.3,29.2)	705	(0,0)
	Gujarat	16,385	26,345	26,285	25,075	23,385	22,225	21,440	9,960	14,355	(-10,10)	70.9%(-19.7,17.6)	15,125	(-5,5)	47.8%(-18.3,17.4)	26,345	(0,0)
	Haryana	6,010	6,810	6,780	6,670	6,130	6,130	4,820	800	3,710	(0,0)	74.7%(-24.8,17.2)	3,910	(0,0)	47.0%(-26.6,37.6)	6,810	(0,0)
	Himachal Pradesh	30	30	30	30	30	30	0	0	30	(0,0)	100.0% (0.0,0.0)	30	(0,0)	100.0% (0.0,0.0)	30	(0,0)
	Jharkhand	8,213	15,856	15,496	14,556	14,011	13,074	12,616	7,643	8,645	(-2,4)	75.6%(-50.8,21.3)	9,104	(-3,4)	57.8%(-28.8,32.3)	15,856	(0,0)
	Karnataka	8,950	13,330	13,330	13,330	12,910	11,810	10,465	4,380	7,265	(-15,10)	73.3%(-18.1,26.7)	7,653	(-3,2)	54.5%(-12.3,16.7)	13,330	(0,0)
	Madhya Pradesh	18,618	27,298	27,298	26,858	25,358	23,558	21,215	8,680	14,879	(-6,4)	73.5%(-18.8,10.3)	15,673	(-13,12)	52.9% (-7.6,5.0)	27,298	(0,0)
	Maharashtra	26,460	29,650	29,650	28,750	25,940	23,620	22,350	3,190	16,151	(-3,6)	81.8% (-8.5,11.6)	17,016	(-4,7)	54.3% (-15.9,7.7)	29,650	(0,0)
	Odisha	15,384	29,684	29,414	29,414	28,486	26,704	22,089	14,300	16,169	(-11,9)	90.2% (-11.2,9.8)	17,044	(-11,6)	68.0%(-19.7,20.9)	29,684	(0,0)
	Punjab state	6,550	6,550	6,550	6,100	5,260	4,420	4,170	0	3,570	(0,0)	72.6%(-23.6,27.4)	3,760	(0,0)	49.9%(-21.4,21.4)	6,550	(0,0)
	Rajasthan	9,574	14,034	13,909	13,909	13,269	12,809	10,315	4,460	7,644	(-4,3)	79.1%(-16.9,20.9)	8,058	(-3,4)	62.2%(-21.3,22.2)	14,034	(0,0)
	Tamil Nadu	11,276	24,086	23,586	23,036	21,776	20,096	19,336	12,810	13,122	(-2,3)	78.5%(-12.7,13.5)	13,824	(-1,1)	55.6%(-16.7,13.0)	24,086	(0,0)
	Telangana	7,135	15,535	15,295	14,753	12,563	12,033	11,426	8,400	8,464	(-2,1)	85.2% (-15.9,5.4)	8,915	(-5,11)	54.8%(-16.6,11.1)	15,535	(0,0)
	Uttar Pradesh	21,850	35,670	35,386	34,622	29,261	26,520	24,370	13,820	19,439	(-8,8)	78.9% (-9.7,8.6)	20,475	(-3,5)	56.5%(-11.8,13.9)	35,670	(0,0)
	Uttarakhand	43	43	43	43	43	43	43	0	43	(0,0)	100.0% (0.0,0.0)	43	(0,0)	100.0% (0.0,0.0)	43	(0,0)
	West Bengal	13,807	14,467	13,936	13,936	12,231	8,917	6,110	660	7,879	(-1,2)	80.4%(-17.3,13.2)	8,303	(-1,1)	62.1%(-27.3,23.8)	14,467	(0,0)

Table S2. Historical Average Capacity Factors of Coal-Fired Power Plants in the States of India, Provinces of China, and Other Countries.

Country	Province	Average Capacity Factor	Reporting Year
Bangladesh[6]	-	0.387	Fiscal Year 2016
Cambodia[7]	-	0.603	2015
Laos[8]α	-	0.996	2016
Mongolia[9]	-	0.645	2014
Myanmar[10,11]	-	0.114	2014
Pakistan[12]β	-	0.116	2015
South Korea[13]	-	0.900	2015
Thailand[14]β	-	0.752	2016
Vietnam[12]β	-	0.399	2015
China[15]γ	Taiwan	0.778	2016
	Shandong	0.592	2016
	Jiangsu	0.581	2016
	Guangdong	0.422	2016
	Inner Mongolia	0.517	2016
	Henan	0.440	2016
	Shanxi	0.434	2016
	Zhejiang	0.448	2016
	Anhui	0.512	2016
	Hebei	0.568	2016
	Xinjiang	0.480	2016
	Liaoning	0.494	2016
	Shaanxi	0.513	2016
	Guizhou	0.454	2016
	Fujian	0.361	2016
	Hubei	0.455	2016
	Hunan	0.373	2016
	Shanghai	0.412	2016
	Guangxi	0.343	2016
	Ningxia	0.560	2016
	Heilongjiang	0.448	2016
	Gansu	0.412	2016
	Jiangxi	0.521	2016
	Jilin	0.375	2016
	Sichuan	0.242	2016
	Yunnan	0.219	2016
	Tianjin	0.492	2016
	Chongqing	0.372	2016
	Beijing	0.493	2016
	Hainan	0.484	2016
	Qinghai	0.455	2016
	Tibet	0.009	2016

India[16]	Delhi	0.024	2016
	Haryana	0.033	2016
	Himachal Pradesh	0.000	2016
	Jammu and Kashmir	0.000	2016
	Punjab	0.034	2016
	Rajasthan	0.052	2016
	Uttar Pradesh	0.054	2016
	Uttarakhand	0.000	2016
	Chhattisgarh	0.049	2016
	Goa	0.000	2016
	Gujarat	0.051	2016
	Madhya Pradesh	0.051	2016
	Maharashtra	0.038	2016
	Andhra Pradesh	0.057	2016
	Karnataka	0.047	2016
	Kerala	0.004	2016
	Puducherry	0.000	2016
	Tamil Nadu	0.050	2016
	Telangana	0.060	2016
	Andaman Nicobar	0.048	2016
	Bihar	0.051	2016
	Damodar Valley Corporation	0.039	2016
	Jharkhand	0.048	2016
	Orissa	0.056	2016
	Sikkim	0.000	2016
	West Bengal	0.048	2016
	Arunachal Pradesh	0.000	2016
	Assam	0.042	2016
	Manipur	0.000	2016
	Meghalaya	0.000	2016
	Nagaland	0.000	2016
	Tripura	0.000	2016

$^{\alpha}$ Only one coal-fired power plant (Hongsa) exists in Laos. Units 1&2 began operation at the end of 2015 and unit 3 began operation in 2016. We used the target total net generation for 2016 for unit 1&2 to calculate an approximate capacity factor.

$^{\beta}$ Because the data source only has electricity generation, we calculated capacity factor by dividing the electricity generation by the total installed capacity until the reporting year in the GCPT17 dataset[1].

$^{\gamma}$ The data did not distinguish between fuels for thermoelectric generation, and thus contains a small part of natural gas power plants.

Table S3. Percentage of Coal-Fired Power Plants that Share a 5 arcmin (~10km) Grid Cell. Note that in this study, we assumed that competition only exists between power plants within the same grid cell (section 2.3). The numbers in parentheses indicate the range across the random samples.

Unit: %		**By Count**	**By Capacity**
Existing Capacity		97.40	98.92
Expanded Capacity		97.62	97.84
Capacity Retirement	1970	97.69	97.85
	1980	97.55	97.74

(decade in which the plant became operational)	1990	97.25	97.53
	2000	96.66	97.01
	2010	94.22	94.13
	2020	91.74	89.12
Regional Transformation	SSP2 1.5°C	72.40 (-0.96, 1.64)	72.09 (-0.75, 1.04)
	SSP2 2°C	73.39 (-0.31, 0.44)	73.46 (-0.65, 0.82)
	SSP2 3°C	87.89 (-0.24, 0.39)	87.51 (-0.09, 0.05)

Table S4. Regional Median Water Withdrawal Intensity. We used median, instead of the mean or capacity-weighted mean, to prevent the undue influence of power plants with once-through power systems, whose water withdrawal intensities are more than ten times that of power plants with wet cooling towers.

Unit: m^3/MWh		**Historical**	**1.5°C**	**2.0°C**	**3.0°C**
Existing Capacity		2.78	2.78	2.78	2.79
Expanded Capacity		-	2.78	2.78	2.78
Capacity Retirement (decade in which the plant became operational)	1970		2.63	2.63	2.64
	1980		2.58	2.58	2.58
	1990		2.53	2.53	2.54
	2000		2.52	2.52	2.52
	2010		2.78	2.78	2.78
	2020		2.56	2.56	2.57
Regional Transformation	SSP2 1.5°C		4.67		
	SSP2 2°C			4.10	
	SSP2 3°C				3.02

3 Estimating the Water Withdrawal Intensities of Coal-Fired Power Plants

3.1 Cooling Water Withdrawal Intensities

We estimated the cooling water withdrawal intensities (m^3/MWh) for once-through (WI_{ot}) and cooling tower (WI_{rc}) systems using previous heat and water balance models.[17] Eq. (S1) and Eq. (S2) show the final formulas that we re-arranged from the original study, and readers are referred therein for the details about their derivation.[17] Table S5 lists the abbreviations in Eq. (S1) and Eq. (S2). The ambient wet-bulb temperature, humidity ratios and enthalpies of inlet and outlet air to the cooling tower are calculated from ambient air temperature, relative humidity, and surface pressure. For the choice of parameters in Eq. (S1) and Eq. (S2), we combined the sources summarized in the original study[17] with other Asian-specific sources, and the details are described below in sections 3.1.1 and 3.1.2.

$$WI_{ot} = \frac{1-\eta_{net}-k_{os}}{\eta_{net}} \frac{1}{\rho_w C_p \max(\min(Tl_{max}-T_w, \Delta Tl_{max}), 0)} \tag{S1}$$

$$WI_{rc} = \frac{1-\eta_{net}-k_{os}}{\eta_{net}} \frac{\omega_{out}-\omega_{in}}{\rho_w\left[\left(h_{a,out}-h_{a,in}\right)\left(1-\frac{1}{n_{cc}}\right)+\left(\frac{T_{wb}+T_{app}}{n_{cc}}-T_w\right)C_p(\omega_{out}-\omega_{in})\right]} \tag{S2}$$

Table S5. Abbreviations in the Cooling System Models.

Notation	Meaning
C_p	Heat capacity of water (4.184 J/g/°C)
$h_{a,in}$	Enthalpy of air entering the tower. Calculated from ambient temperature and ω_{in}
$h_{a,out}$	Enthalpy of air exiting the tower. Calculated from ambient temperature and ω_{out}
k_{os}	Fraction of heat loss through flue gas and (negligible amount) other dissipative losses
n_{cc}	Cycles of concentration of the cooling water
T_{app}	Approach of the cooling tower (i.e. the difference between ambient wet bulb temperature and the cooled water temperature)
Tl_{max}	Maximum permissible temperature of the discharged cooling water (°C)
T_w	Temperature of the intake water (°C)
T_{wb}	Ambient wet-bulb temperature. Calculated from ambient temperature and pressure
WI_{ot}	Water withdrawal intensity for once-through cooling system (m^3/MWh)
WI_{rc}	Water withdrawal intensity for recirculating cooling system (m^3/MWh)
ΔTl_{max}	Maximum permissible rise in cooling water temperature in the condenser (°C)
η_{net}	Net thermal efficiency of the power plant (i.e. the ratio of the net electricity generation to the heat input from fuel)
ρ_w	Density of water (1000 kg/m)
ω_{out}	Humidity ratio of air exiting the tower. Assumed to equal the saturation humidity ratio at ambient atmospheric pressure and temperature
ω_{in}	Humidity ratio of air entering the tower. Assumed to equal ambient humidity ratio

3.1.1 Thermal Efficiency under Wet and Dry Cooling (η_{net}) and Flue Gas Loss (k_{os})

Figure S19 shows the thermal efficiencies calculated from the heat rates for different combustion technologies and size of coal-fired power plants reported in the GCPT17 dataset.[1] The GCPT17 thermal efficiencies do not reflect any decrease in thermal efficiency with decreasing size of power plants. Therefore, we also tested a set of thermal efficiencies that previous studies derived from solving the Rankine cycles of existing thermal power plants.[2,3] Figure S20 shows the relationships between nameplate capacity and this second set of thermal efficiencies for existing coal-fired power plants in Asia. The second set of thermal efficiencies did not distinguish circulating fluidized bed (CFB) and integrated gasification combined cycle (IGCC) from the other technologies. Therefore, we set the thermal efficiencies of CFB power plants to be the same as subcritical power plants, and the thermal efficiencies of IGCC power plants to be the same as supercritical power plants, because their thermal efficiencies were similar in literature reports, respectively (Table S6). The second set of thermal efficiencies also did not contain IGCC power plants with CO_2 capture and storage (CCS). Therefore, we used the median value from literature reports for the IGCC-CCS power plants (31.8% from Table S6).

For sensitivity analysis, we varied the flue gas loss parameter between 6%, 12%, and 25% uniformly across all the power plants, based on the range of variability found in past.[18–20]

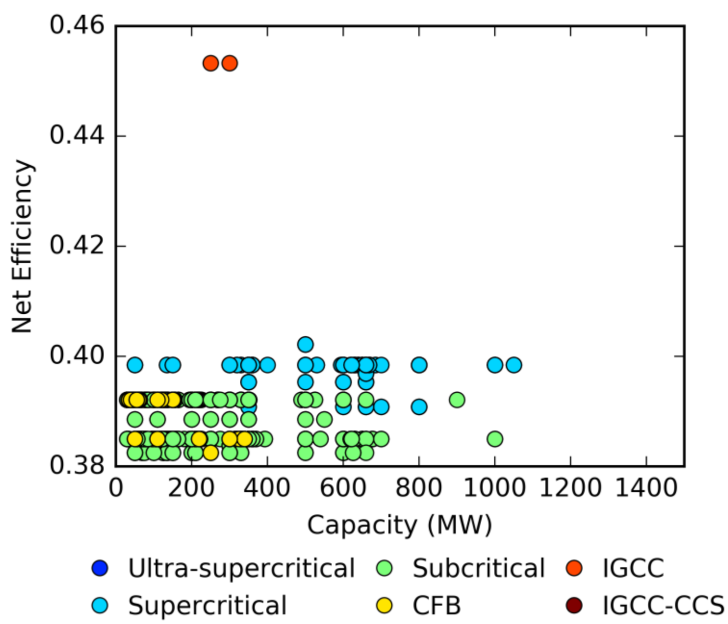

Figure S19. Thermal Efficiencies of the Existing and Planned Coal-Fired Power Plants in East, Southeast, and South Asia for Different Combustion Technologies from the GCPT17 Dataset.[1] Abbreviations: CFB–circulating fluidized bed; IGCC–integrated gasification combined cycle; CCS–CO_2 capture and storage.

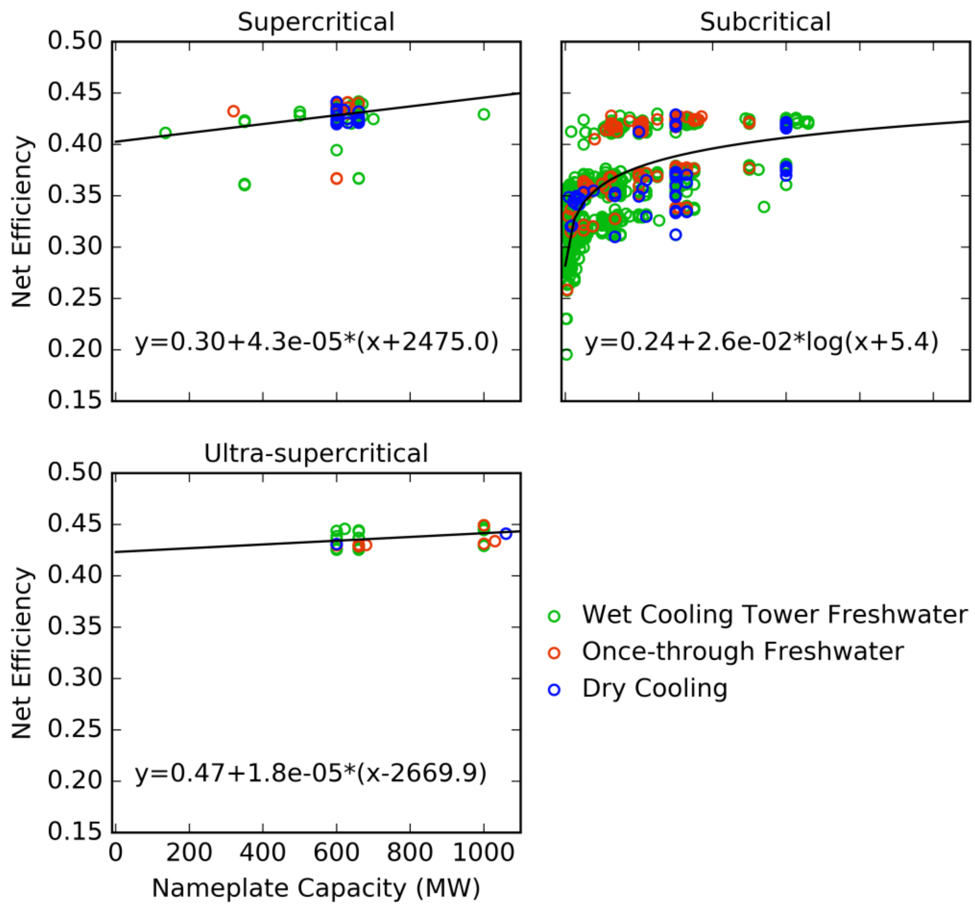

Figure S20. Relationship between Mean Annual Thermal Efficiencies for the Coal-Fired Power Plants in East, Southeast, and South Asia from the GCPT17 Dataset,[1] for Different Combustion Technologies and Cooling Systems. Previous studies have estimated the mean annual thermal efficiencies by solving the Rankine cycle,[2,3] and the dataset was matched to the GCPT17 dataset using location and names of the power plants. Lines: fitted relationships between thermal efficiencies and nameplate capacity for different combustion techniques (the different cooling systems were pooled together because not enough data points are available for dry cooling).

Table S6. Literature-based Thermal Efficiencies of Different Combustion Technologies for Coal-Fired Power Plants. Note: the thermal efficiencies from reference[21] distinguished between wet- and dry-cooling; the wet-cooling values are shown here.

Technology	Thermal Efficiency
IGCC	44% [22]; 39-42.1% [23]
Subcritical	38.2% [22]; 36-40% [21]
Supercritical	41% [24]; 41-43% [22]; 37-42% [21]
Ultra-supercritical	45.19% [22]; 40-46% [21]
Circulation Fluidized Bed (CFB)	38.0-38.9% [25]; 35-40% [21]
IGCC/CCS	31.0-32.6% [23]

3.1.2 Parameters Related to the Cooling Systems

Table S7 compares the chosen values for the cooling system-related parameters in Table S5 between the original study[17] and this study. We used the same range of temperatures for the approach of the cooling tower (T_{app}) as the original study, because few Asian-specific literature reported these parameters, and internet search for the design specifics of cooling tower suppliers supported the range of values in the original study. We tested two slightly lower values (3 and 5) and a much higher value (20) for the cycles of concentration (n_{cc}) than the original study. The lower values were chosen because the Chinese regulation on water use by thermal power plants requires the cycle of concentration to be 3-5.[26] The high value was chosen because the regulation notes that thermal power plants in water-scarce regions or using intake water sources that have low dissolved solids can use higher cycles of concentration, and some coal-fired power plants in the arid region of other countries have used high cycles of concentration (14 to 39).[18,26]

Table S7. Comparison between the Parameters Cooling System in the Original Study[17] and this Study.

Parameter	Source Study	This Study
Approach of the cooling tower ($\boldsymbol{T_{app}}$)	4-8	4, 6, 8
Cycles of concentration (n_{cc})	3-6	3, 5, 20
Maximum permissible temperature of the discharged cooling water (Tl_{max})	EIA Form 923; 32°C if no data exists	Vary by country or sub-country region
Maximum permissible rise in cooling water temperature in the condenser (ΔTl_{max})	EIA Form 923	3°C, 10°C, 25°C

The maximum permissible temperature of the discharged cooling water (Tl_{max}) depends on the physical properties of the receiving water body and the thermal tolerance of local aquatic species. We reviewed the regulations for various Asian regions. The "National Technical Regulation on Industrial Wastewater" of Vietnam requires 40°C.[27] The Effluent Standard of Taiwan requires 38°C during May-September and 35°C during October-April.[28] The design code for fossil-fuel power plants in China requires that the temperature of thermal effluents from once-through cooling systems do not exceed the 90th percentile of the observed daily summer (June, July, August) water temperature.[29] The "General Standards for Discharge of Environmental Pollutants" of India requires ≤5°C above the receiving water body's temperature.[30] We applied each of these regulations to the respective country or sub-country region, applied the Vietnam standard on the other Southeast Asian countries (Myanmar, Thailand, Laos, and Cambodia) because of geographical proximity, and applied the Indian standard on Bangladesh because of geographical proximity.

The maximum permissible rise in cooling water temperature in the condenser (ΔTl_{max}, also called the condenser range) depends on the materials and design of the condenser. Typical designed condenser ranges are between 5.6 and 14ºC, but empirical data in the United States suggested that actual condenser ranges varied between 0.6 and 26ºC.[31] Low actual condenser ranges occurred more often at power plants that have low heat rejection rates to the condenser,[31] which suggests that low condenser ranges like 0.6ºC reflect operational decisions rather than lack of tolerance to thermal stress by those condensers. Therefore, we varied the condenser range between the levels 5ºC, 14ºC, and 25ºC to capture the range of uncertainty in this parameter. The same condenser range was applied uniformly across the power plants due to lack of more detailed information.

3.2 Non-Cooling Water Use at the Coal-Fired Power Plants

Coal power plants may require considerable amounts of water for non-cooling processes, including flue-gas desulfurization (FGD), ash handling, boiler makeup, service and drinking water for humans at the site of the plant. This study ignores service and drinking water, because they are likely supplied from municipal sources. The volume of boiler makeup water is negligible compared to cooling water.[23] FGD and ash handling may or may not use a significant amount of water, depending on whether the plant uses wet or dry technologies, and whether the plant recycles blowdown water from the cooling system for these processes.[23] Therefore, we considered two extreme cases: (1) FGD and ash handling processes do not have water withdrawal, because they use dry technologies or entirely use internally recycled water from the cooling system, and (2) FGD and ash handling processes have additional water withdrawals that are 100%-added to the cooling water withdrawals.

For wet FGD, previous study based on Illinois No.6 bituminous coal (2.82% sulfur content based on dry weight) suggests that the water requirement is 0.37-0.46m^3/MWh.[23,32] Coals in China and India have relatively low sulfur content.[33,34] Therefore, we took the lower value, 0.37m^3/MWh, as an approximation.

We calculated the water requirement of wet ash handling (WI_{ash}, m^3/MWh) as a function of the gross heat rate (GHR, J/MWh), net calorific value (NCV, J/kg), ash content (A, % based on mass), water-to-ash ratio of the slurry (λ, % based on mass), and the density of water (ρ_w, 1000 kg m^{-3}) using Eq. (S3):

$$WI_{ash} = \frac{GHR}{NCV} \times A \times \lambda \times \frac{1}{\rho_w} \tag{S3}$$

The gross heat rate is related to net thermal efficiency (η_{net}) via:

$$GHR = \frac{3.6 \times 10^9 \text{ J MWh}^{-1}}{\eta_{net}(1+8\%)} \tag{S4}$$

, assuming 8% auxiliary power consumption.[35]

The η_{net} in Eq. (S4) are from the GCPT17 dataset[1] and previous estimations based on the Rankine cycle[2,3] like section 3.1.1. Table S8 summarizes the values of NCV and A used in this study for the coal-fired power plants in different regions. The values for power plants in India are the weighted averages of different grades of non-coking coal-fired based on the dispatched amounts of each grade in India during 2012-2016.[36–39] The values for power plants in China are based on previous studies.[40,41] Due to a lack of data, the values for the other countries are the average of China and India. For water-to-ash ratio of the slurry, we assume 28% ash concentration (mass/mass), which translates to a water-to-ash ratio of 2.6.[42]

Table S8. The Net Calorific Values and Ash Contents Used for Power Plants in China, India, and Other Asian Countries in this Study.

Country	Net Calorific Value (J/kg)	Ash Content (%)
China	2.3012*10^7 J/kg	21.7%
India	4500 1.8828*10^7 J/kg	36%
Other	5000 2.0920*10^7 J/kg	28%

Apart from FGD and ash-handling, two of the planned power plants in the GCPT17 dataset[1] plan to use IGCC with CCS technology. CCS at IGCC power plants requires the use of shift reactor, where steam is supplied to convert carbon monoxide in the syngas to carbon dioxide and to produce more hydrogen. The additional water use intensity for shift steam is 0.24-0.40m^3/MWh according to previous simulation results.[23] We used the average value, 0.32m^3/MWh, in this study.

4 Sensitivity Analysis and Validation of the Modeled Water Withdrawal Intensities

We compared the modeled water withdrawal intensities under the above-described different choices of parameter values to previously surveyed water withdrawal intensities at coal-fired power plants that use once-through and cooling tower systems in China and India.[43,44] The Chinese study included more than 300 plants, while the Indian study only included one supercritical plant and five subcritical plant of unknown sizes and using wet-cooling towers, and did not report water withdrawal for any once-through plants.[43,44] Figure S21 together with Table S9 and Table S10 show the results of the comparison. The "baseline" parameter choice (number 1 on the *x*-axes in Figure S21) is to use the GCPT17 dataset for thermal efficiency, assume zero non-cooling water use, and the median values in Table S7 for all the other parameters. Each of the other parameter choices in Figure S21 differs from number 1 by the value of one parameter. The boxplots for the modeled values in Figure S21 are based on the pool of median water withdrawal factors of the existing coal-fired power plant in the study region during the historical period (1950-2005, using forcing from the GFDL-ESM2M global climate model), and therefore only reflects the spatial variation in water withdrawal intensities. The water withdrawal intensity of cooling tower only varies slightly with meteorological conditions and water temperature. The water withdrawal intensity of once-through cooling increases rapidly with water temperature, but the surveyed water withdrawal intensities do not provide water temperature information.[43,44] Therefore, we assumed that the surveyed water withdrawal intensities reflected days with median water temperature. Differences in the boxplots between the climate models (see Table 1 in the main text for the list of climate models used in this study) were negligible.

The surveyed water withdrawal intensities[43,44] of coal-fired power plants were higher in India than in China (Figure S21). This difference between China and India is reasonable, because the Indian plants operate at lower efficiency and does not fully recycle wastewater.[45]

For the coal-fired power plants with cooling towers in China, parameter choice 2, which uses the estimated thermal efficiencies from Rankine cycle,[2,3] performs the best for the plants ≤350MW, while parameter choice 1, which uses the thermal efficiencies from the GCPT17 dataset,[1] performs the best for the plants >350MW (Figure S21). For the coal-fired power plants with cooling towers in India, parameter choice 5 gives the closest agreement with the literature-reported values, even though it still overestimates the water withdrawal intensities for the plants >550MW (Figure S21). For the coal-fired power plants with once-through cooling, parameter choices 1 and 5 result in overestimations in the water withdrawal intensities of ultra-supercritical plants at 950-1050MW, while parameter choice 2 performs well (Figure S21). Based on these results, we used parameter choice 2 for the plants ≤350MW in China, parameter choice 1 for the plants >350MW in China, and parameter 5 for the plants in India. We used the same parameter choices for the power plants using wet cooling towers and once-through cooling for consistency. For the plants in other countries than China or India, we used the same parameter as China to prevent over-estimation of water withdrawal intensities.

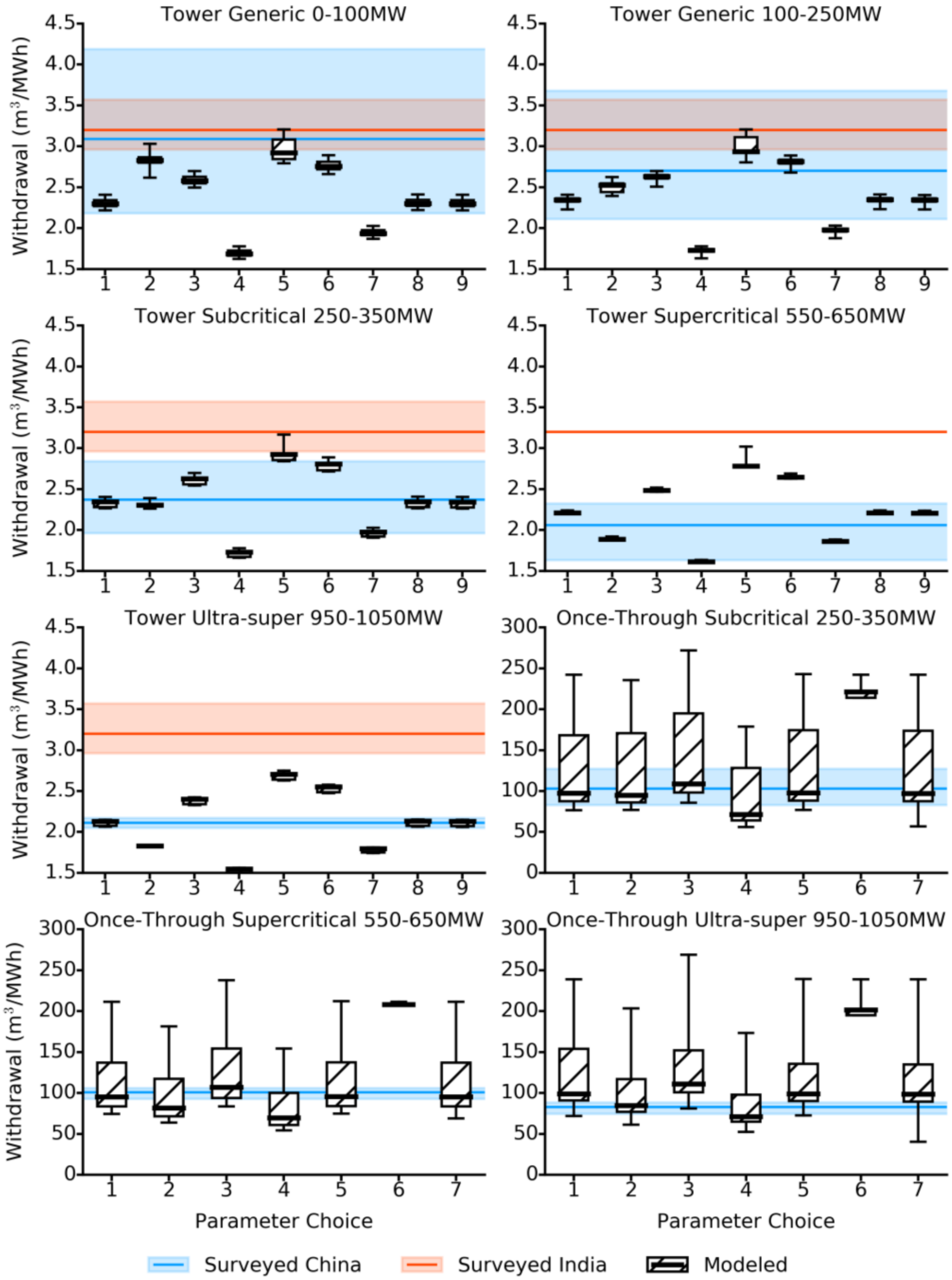

Figure S21. Comparison between Surveyed Water Withdrawal Intensities for Coal-Fired Power Plants in China and India[43,44] and Modeled Water Withdrawal Intensities in the Study Region for Different Cooling Systems, Combustion Technologies, and Unit Sizes. Shaded regions indicate the ranges of surveyed values. Boxplots show the quartiles, minimum, and maximum of modeled values. The numbered parameter choices are explained in Table S9 and Table S10. The generic type included all types of combustion technologies that have the indicated cooling system and unit sizes.

Table S9. Numbered Parameter Choices for Power Plants with Once-through Cooling Systems. The abbreviations for cooling water use model parameters are the same as in Table S5. The numbering refers to the numbering on the *x*-axes of Figure S21.

Number	Source for η_{net}	k_{os}	Add non-cooling water use	ΔTl_{max}
1	GCPT17	0.12	No	10°C
2	Estimates based on Rankine cycle[2,3]	0.12	No	10°C
3	GCPT17	0.06	No	10°C
4	GCPT17	0.25	No	10°C
5	GCPT17	0.12	Yes	10°C
6	GCPT17	0.12	No	3°C
7	GCPT17	0.12	No	25°C

Table S10. Numbered Parameter Choices for Power Plants with Wet Cooling Tower Systems. The abbreviations for cooling water use model parameters are the same as in Table S5. The numbering refers to the numbering on the *x*-axes of Figure S21.

Number	Source for η_{net}	k_{os}	Add non-cooling water use	n_{cc}	T_{app}
1	GCPT17	0.12	No	5	6°C
2	Estimates based on Rankine cycle[2,3]	0.12	No	5	6°C
3	GCPT17	0.06	No	5	6°C
4	GCPT17	0.25	No	5	6°C
5	GCPT17	0.12	Yes	5	6°C
6	GCPT17	0.12	No	3	6°C
7	GCPT17	0.12	No	20	6°C
8	GCPT17	0.12	No	5	4°C
9	GCPT17	0.12	No	5	8°C

5 Sensitivity of the Usable Capacity (*UC*) and Usable Capacity Factor (*UF*) to Environmental Flow Methods and Minimum Load Levels

The availability of streamflow to the coal-fired power plants depends on many factors, including water demand from other users, national and local water allocation policies, and environmental flow requirements. The water use of non-thermal power sectors (domestic, agriculture, and other industrial water use) are already reflected in the simulated streamflow of PCR-GLOBWB 2.[46] We further subtracted the environmental flow from the simulated streamflow, and used the remainder as the available streamflow to the coal-fired power plants. Because local water allocation policies are unknown, we allocated the available streamflow to each coal-fired power plant proportional to its nameplate capacity, when multiple power plants are in the same 5 arcmin grid of the hydrological model.

To determine the appropriate method to calculate environmental flow is somewhat difficult, because environmental flow standards either do not exist in the study region, or consist of annual values that do not reflect the timing of flow, which is an essential component of environmental flow.[47–50] In addition, the calculation of environmental flow should ideally incorporate information on flow-ecology relationships and socio-economic needs, but such information are not available at the level of spatial coverage of this study.[50,51] With these limitations in mind, we compared three hydrological environmental flow methods that have been previously applied at large scale:[52–54] the annual flow quantiles method ($Q_{90}\_Q_{50}$), the variable monthly flow method (VMF), and the shifted flow-duration-curve method (ShiftFDC), which have previously been applied at large scale.[52–54] The $Q_{90}\_Q_{50}$ and VMF methods were developed for use at global scale, and they out-performed other methods in reproducing the results of small-scale environmental flow studies.[52] The ShiftFDC method was developed for South Asia and has been applied to India and Nepal.[53,54] The ShiftFDC method requires choosing the environmental management class (EMC) of each river between A-F beforehand.[53,54] Higher EMC means that a river is more severely modified and requires less environmental flow.[53,54] In a prior assessment, EMC “C” was assumed for the rivers in India.[54]

A thermal electricity generation unit cannot operate effectively if its *UF* is below some minimum load level, typically 20-50%, depending on the design of the generation process.[55] Therefore, we also tested two minimum load levels (20% and 50%), below which we set the *UF* of each generation unit in each power plant to zero.

Figure S22 compares the actual coal-fired power generation to the potential amount of electricity that can be generated per year (i.e. annual average *UC* times the number of hours per year) at the existing coal-fired power plants in four countries under different choices of environmental flow methods and minimum load levels.[55] The actual coal-fired power generation are from reported annual electricity generation from China, India, Vietnam, and Pakistan for 2010-2014.[12,56] Since some existing plants are not covered by the simulations of PCR-GLOBWB 2 (Figure S1), we adjusted the actual electricity generation by removing the potential electricity generation of the coastal power plants assuming they operated at 100% capacity, and excluded the Inner Mongolia, Heilongjiang, Liaoning, and Jilin provinces from China's actual electricity generation. The provincial-level data for Inner Mongolia, Heilongjiang, Liaoning, and Jilin did not distinguish between natural gas and coal-fired power plants.[56] But the capacity of natural gas power plants only comprises about 5% of the thermal generation capacity in China, and 89% of the natural gas power plants are in Beijing, Tianjin, or the southeastern provinces.[57] Therefore, the impact of natural gas power plants on Figure S22's comparison should be small.

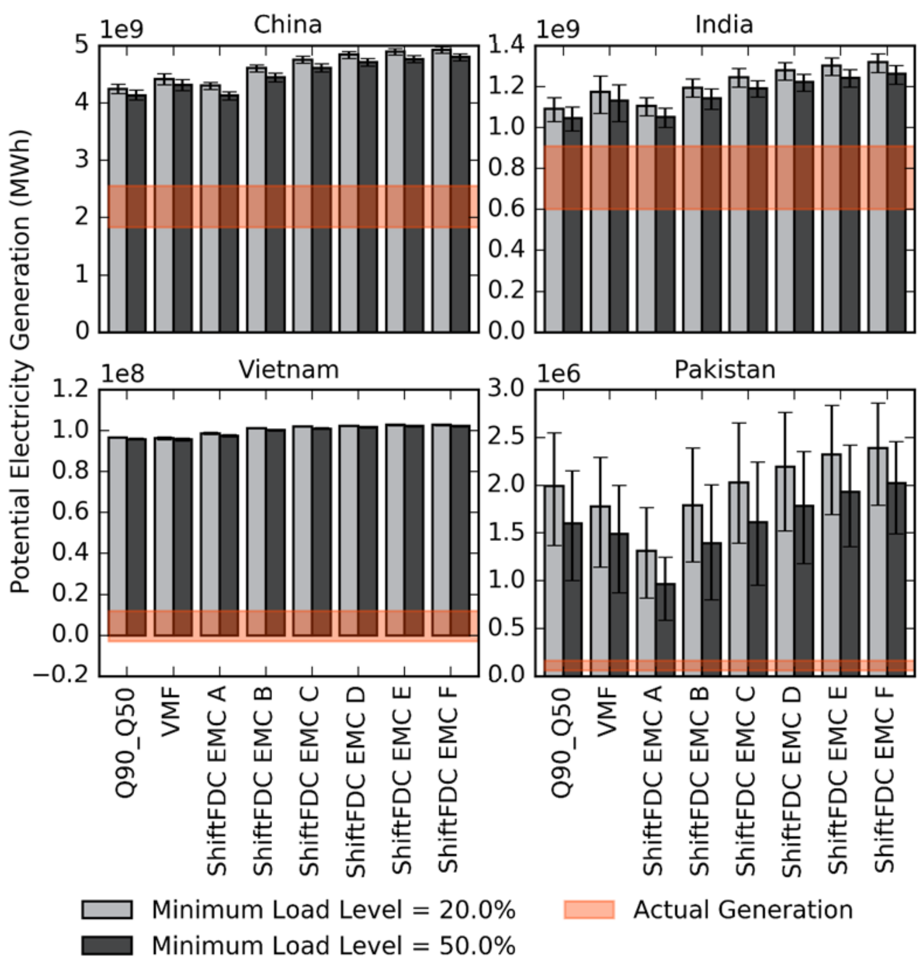

Figure S22. Comparison between the Annual Observed National Coal-Fired Power Generations during 2010-2014 and the Simulated Mean Annual Potential Electricity Generations at the Existing Coal-Fired Power Plants under Different **Environmental Flow Methods and Minimum Load Levels during 1950-2005.** Shaded regions show the range of observations. The bars show the average values of the five global climate models, and the whiskers show the maximum and minimum values.

All the environmental flow methods and minimum load levels yielded larger potential electricity generation by the existing coal-fired power plants in the GCPT17 dataset[1] than the actual coal-fired power generation in the compared countries (Figure S22), implying that non-streamflow factors limited the actual electricity generation. As such, the actual electricity generation cannot inform the choice of environmental flow method or minimum load level. We chose to use the ShiftFDC method with EMC "C", which gives a medium level of environmental flow, and the lower minimum load level (20%), in the main text.

As sensitivity analyses, the impacts of environmental flow method and minimum load level on the historical (1950-2005) annual average *UF*s, and on the changes in annual average *UF*s from the historical period to the 2°C scenario of climate change are shown in Figure S23 and Figure S24 at plant level. Changes in the environmental flow method can considerably change the *UF*s (Figure S23). If the highest EMC ("A") is used, the *UF*s of some power plants decrease by as much as 50% compared to the EMC "C". If the lowest EMC ("F") is used, the *UF*s of some power plants increase by as much as 50%. The impacts of the minimum load level on the historical annual average *UF*s of the power plants are smaller (<10%).

Changes in the environmental flow method and minimum load level can also impact the changes in annual average *UF*s from historical to the 2°C scenario of climate change, but the impacts are smaller than on the historical annual average *UF*s (Figure S24). The main differences are between the three types of environmental flow methods ($Q_{90}\_Q_{50}$, VMF, and ShiftFDC), while the differences between the EMC's within the ShiftFDC method are small. Using the $Q_{90}\_Q_{50}$ or VMF method enhanced the general spatial pattern of the impacts of climate change on annual average *UF*s compared to the ShiftFDC method. That is, in Southeast Asia and southeastern China, where using the ShiftFDC method with EMC "C" gave negative changes in *UF*s (see Figure 4b in the main text), using the $Q_{90}\_Q_{50}$ or VMF method gave greater negative changes. In northern China and most of South Asia, where using the ShiftFDC method with EMC "C" gave positive changes in *UF*s (see Figure 4b in the main text), using the $Q_{90}\_Q_{50}$ or VMF method gave greater positive changes.

The results of Figure S23 and Figure S24 show that the environmental flow method is a major source of uncertainty in the simulated *UC*s and *UF*s of the power plants, but do not change the broad pattern of the impact of climate change. Future research that focus on smaller regions can refine the environmental flow method based on local information, and obtain more accurate estimates for the absolute level of *UC*s and *UF*s.

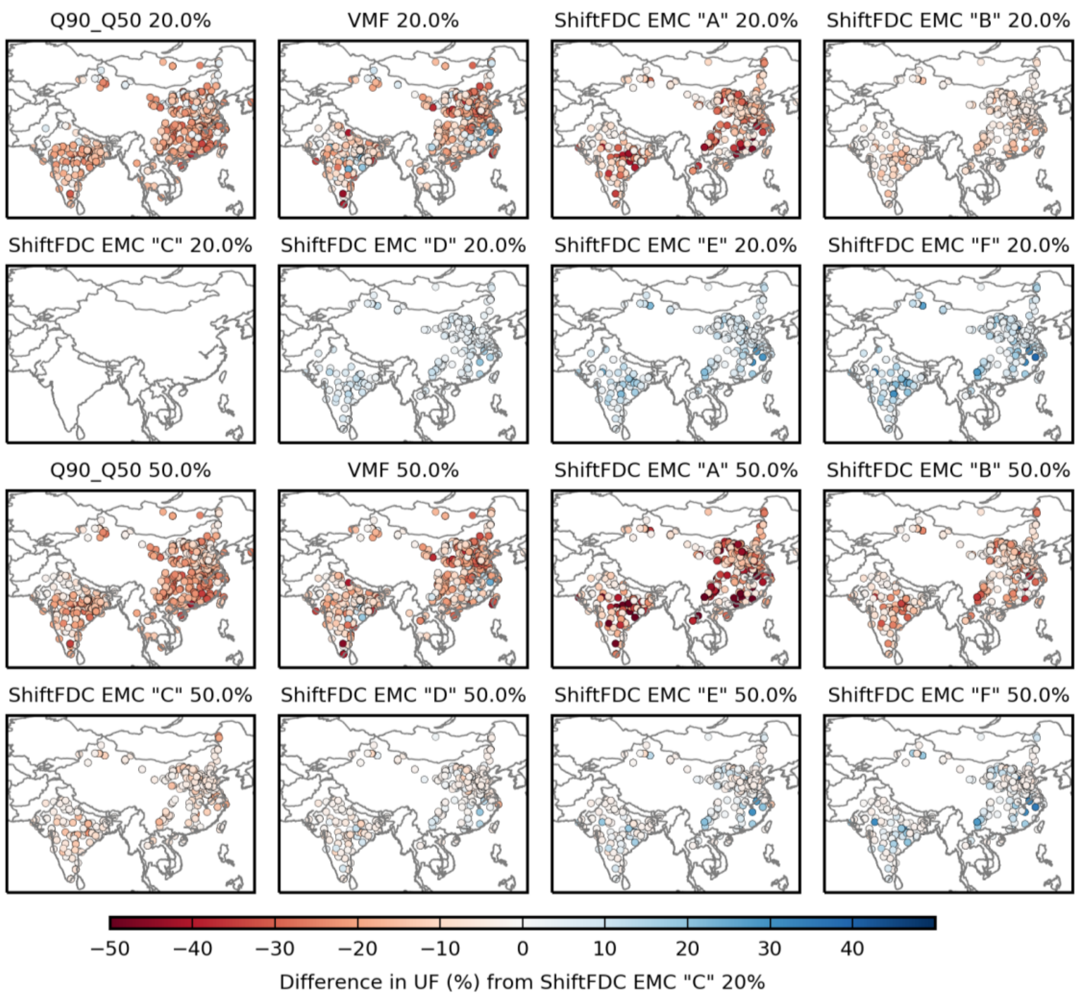

Figure S23. Differences in the Historical (1950-2005) Usable Capacity Factors (*UF*) of the Coal-Fired Power Plants Between Applying Various Combinations of Environmental Flow Method (Q_{50}_Q_{50}, VMF, ShiftFDC with EMC "A" through "F") and Minimum Load Level (20%, 50%) and Applying the Default Combination (ShiftFDC with EMC "C" and a Minimum Load Level of 20%). The power plants where changes are less than 1% are not shown.

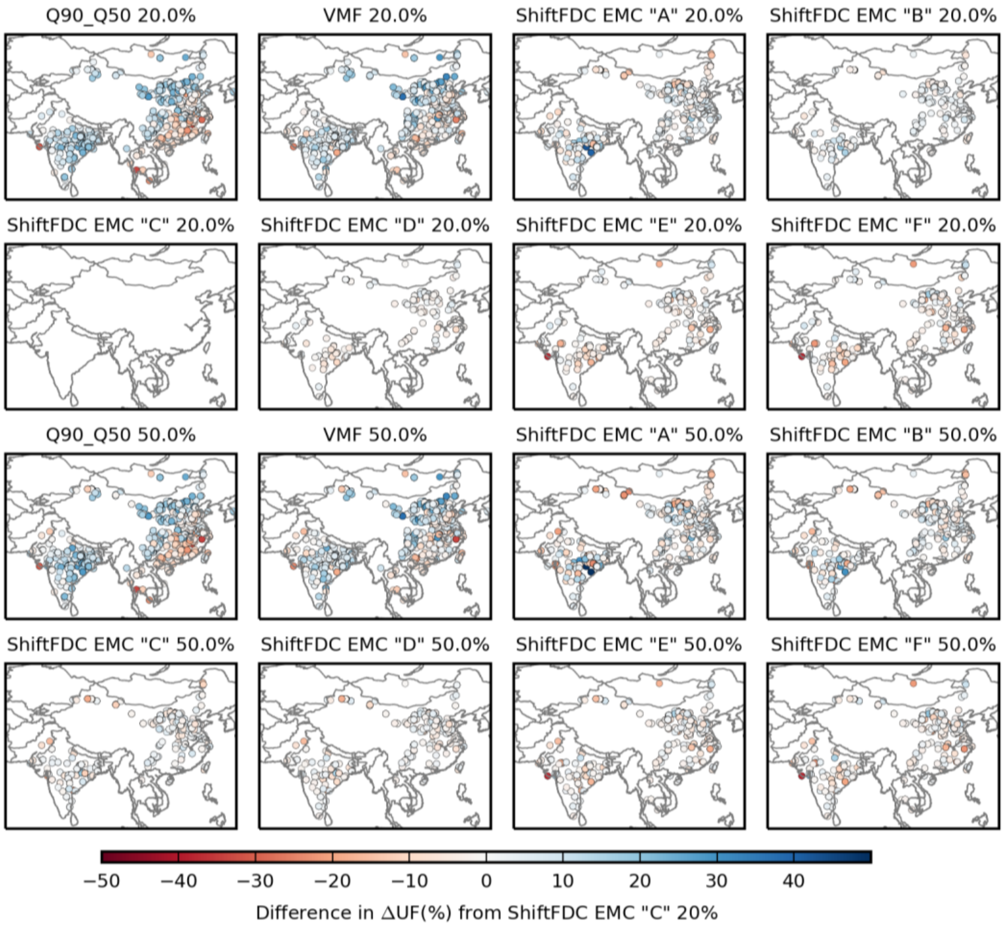

Figure S24. Differences in the Changes in Usable Capacity Factors (*UF*) at Power Plant Level from the Historical Period (1950-2005) to the 2°C Scenario of Climate Change Between Applying Various Combinations of Environmental Flow Method (*Q_{50}_Q_{50}*, VMF, ShiftFDC with EMC "A" through "F") and Minimum Load Level (20%, 50%) and Applying the Default Combination (ShiftFDC with EMC "C" and a Minimum Load Level of 20%). The power plants where changes are less than 1% are not shown.

6 Scenarios of Coal-Fired Power Plants Construction and Retirement under Carbon Emission Mitigation

6.1 ASIA Regional Scenarios

As the 1.5°C, 2°C, and 3°C climate goals are investigated in this study, we designed the scenarios of evolution of the coal-fired power plants ("local scenarios") to be consistent with regional scenarios of energy systems evolution that can achieve these climate goals. We obtained various scenarios of energy systems evolution simulated by different integrated assessment models (IAMs) for the ASIA region from the Shared Socioeconomic Pathway (SSP) database Version 1.1.[58] We used the SSP2 scenarios that lead to global mean temperature increases that are closest to 1.5ºC, 2ºC, 3ºC above the pre-industrial level by 2100 (Figure S25) as the regional level references for the local scenarios in this study, because SSP2 was the socioeconomic scenario used in the hydrological simulations of PCR-GLOBWB 2.

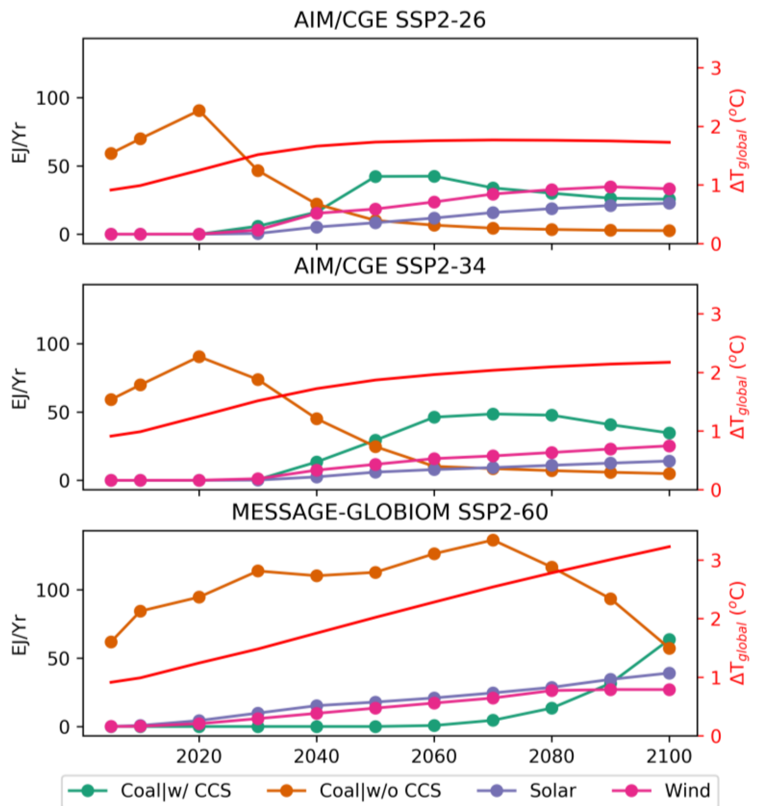

Figure S25. Coal With CO_2 Capture and Storage (CCS), Coal Without CCS, Solar, and Wind Parts of the Primary Energy Mixes in the Selected ASIA Regional Scenarios. The scenarios are from SSP2 IAM simulations that lead to global mean temperature increases closest to 1.5ºC, 2ºC, and 3ºC above pre-industrial levels in 2100. The numbers 26, 34, and 60 indicate the representative concentration pathways (RCP2.6, RCP3.4, and RCP6.0) simulated by the IAM. EJ/Yr: exajoules (10^{18} J/Yr).

The ASIA region in the SSP database is a broad region that covers Asian countries except Japan[1].[58] Therefore, we used a two-step downscaling procedure to translate the ASIA regional scenarios into decisions whether to keep/remove an existing or planned power plant. The first step translates the ASIA regional scenarios to national level scenarios after taking into consideration historical coal-fired electricity generation characteristics for the countries. The second step translates the national level scenarios into individual power plant decisions.

Past studies have downscaled regional socioeconomic scenarios to finer spatial levels using methods that may be broadly classified into algorithmic methods, methods of intermediate complexity, or simulation methods.[59] Among these three choices, simulation method requires large-scale data collection far beyond the scope of this study. Algorithmic methods can be further divided into proportional downscaling, convergence downscaling, and scenario-based downscaling.[59] Proportional downscaling allocates the regional data to finer spatial scales via fixed proportions[60]. Convergence downscaling allocates the regional data to finer spatial scales assuming gradual convergence to the uniform regional level.[60,61] Scenario-based downscaling uses local scenarios that may be available from local studies or constructed with the aid of stakeholders.[62,63] Methods of intermediate complexity use allocation rules that can take into account more local factors than proportional or convergence downscaling.[64–66] Because the target of our downscaling is a binary decision on whether to keep/remove a power plant and whether to simulate the

---

[1] R5.2ASIA = The region includes most Asian countries with the exception of the Middle East, Japan and Former Soviet Union states. Afghanistan, Bangladesh, Bhutan, Brunei Darussalam, Cambodia, China (incl. Hong Kong and Macao, excl. Taiwan) Democratic People's Republic of Korea, Fiji, French Polynesia, India, Indonesia, Lao People's Democratic Republic, Malaysia, Maldives, Micronesia (Fed. States of), Mongolia, Myanmar, Nepal, New Caledonia, Pakistan, Papua New Guinea, Philippines, Republic of Korea, Samoa, Singapore, Solomon Islands, Sri Lanka, Taiwan, Thailand, Timor-Leste, Vanuatu, Viet Nam.

CCS-related water use on it, we used a combination of proportional downscaling, convergence downscaling, and random sampling in our downscaling procedure.

6.2 National Total Installed Coal Capacity

In the first step, the ASIA-level scenarios of coal consumption in EJ/Yr are downscaled to national level in the unit of megawatt coal-fired power generation capacity following the convergence approach. To facilitate the downscaling, we write the historical or future installed capacity of coal in country j, year t ($C_{j,t}$) as Eq. (S5):

$$C_{j,t} = m_{j,t} * P_{j,t} * h_{j,t} / f_{j,t} \tag{S5}$$

, where $m_{j,t}$ is the coal consumption rate (EJ/Yr/million people), $P_{j,t}$ is the population (million people), $h_{j,t}$ is the ratio of coal-fired electricity generation to coal consumption (MWh/EJ), and $f_{j,t}$ is capacity factor of coal power plants (MWh/MW).

Due to limitations in data availability, we applied Eq. (S5) using historical data only for seven major coal consumers (China, India, Taiwan, Vietnam, Mongolia, South Korea, and Japan) and used proxy data for the other countries. The existing and planned coal capacities for all countries in the study region are shown in Table S11. Table S11 also shows that in each country, some coal-fired power plants are outside the coverage of the hydrological simulations. Therefore, after applying Eq. (S5), we scaled the $C_{j,t}$'s using the ratio of the country's total existing and planned capacity inside coverage to total existing and planned capacity inside and outside coverage to obtain the final downscaled installed national coal generation capacity.

Table S11. The Existing and Planned Coal Capacity that are within and Outside the Coverage of the Hydrological Simulations for Countries in the Study Region. Data source: GCPT17.[67]

	Existing Capacity (MW)		Planned Capacity (MW)	
	Inside	Outside	Inside	Outside
Bangladesh	250	0	6820	0
Cambodia	270	100	1040	150
China	776986	144836	227518	21160

India	211482	6574	115853	5930
Japan	780	43464	0	18321
Laos	1878	0	0	0
Mongolia	706	0	8780	0
Myanmar	160	0	550	0
Pakistan	1750	0	10945	300
Philippines	2976	4230	4221	6320
South Korea	18774	15932	9004	3182
Taiwan	8355	7802	3249	1600
Thailand	4023	1434	1606	2200
Vietnam	12377	2594	23825	10050

We obtained the values for the variables in Eq. (S5) is as follows:

1. For the seven selected countries, we calculated historical coal consumption rates ($m_{j,t}$) from historical coal consumption and population data (Figure S26),[68–70] and assume that the future coal consumption rates converge linearly for each country j from the historical value in year 2010 to the ASIA-level coal consumption rate in year 2100 (Figure S27, left). For the other countries, we set the future coal consumption rates of Pakistan and Bangladesh equal to India, and Thailand, Laos, Myanmar, and Cambodia to Vietnam based on geographical proximity.

2. The future population ($P_{j,t}$) for all the countries are from the SSP2 scenario.[71]Figure S27 right hand side shows the future evolution of the coal consumptions ($m_{j,t}*P_{j,t}$) of the seven selected countries**.**

3. The historical coal generation-consumption ratio ($h_{j,t}$), calculated from historical data,[68,72] display convergent trends towards around 70 TWh/EJ for the selected countries except Mongolia (Figure S28). Therefore, we set the future $h_{j,t}$ of Japan, South Korea, India, Taiwan, and Mongolia to be their 2016 values. For the future $h_{j,t}$ of China and Vietnam, we fitted asymptotic curves approaching 70 TWh/EJ and took the 2050 values from the fitted curves (Figure S29). For the other countries, we set the future coal generation-consumption ratios of Pakistan and Bangladesh equal to India, and Thailand, Laos, Myanmar, and Cambodia to Vietnam based on geographical proximity.

4. We assumed that the capacity factors of coal-fired power plants ($f_{j,t}$) of all countries remain constant at historical levels (Table S12). Table S12 does not contain capacity factor for the Philippines, but the coal capacity the Philippines are generally ocean-cooled (Figure S1), and therefore outside the scope of this study.

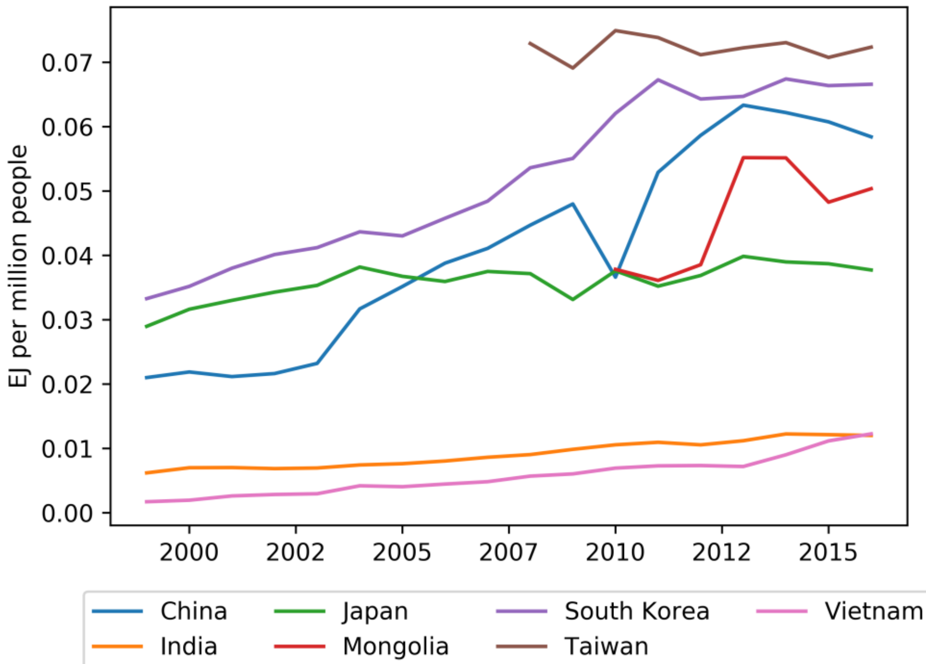

Figure S26. The Historical per Million Capita Coal Consumption of Selected Major Coal Consumers. Data sources: the Coal Information 2001-2018 of the International Energy Agency,[68] the World Bank population,[70] and population from the Statistical Bureau of Taiwan.[69]

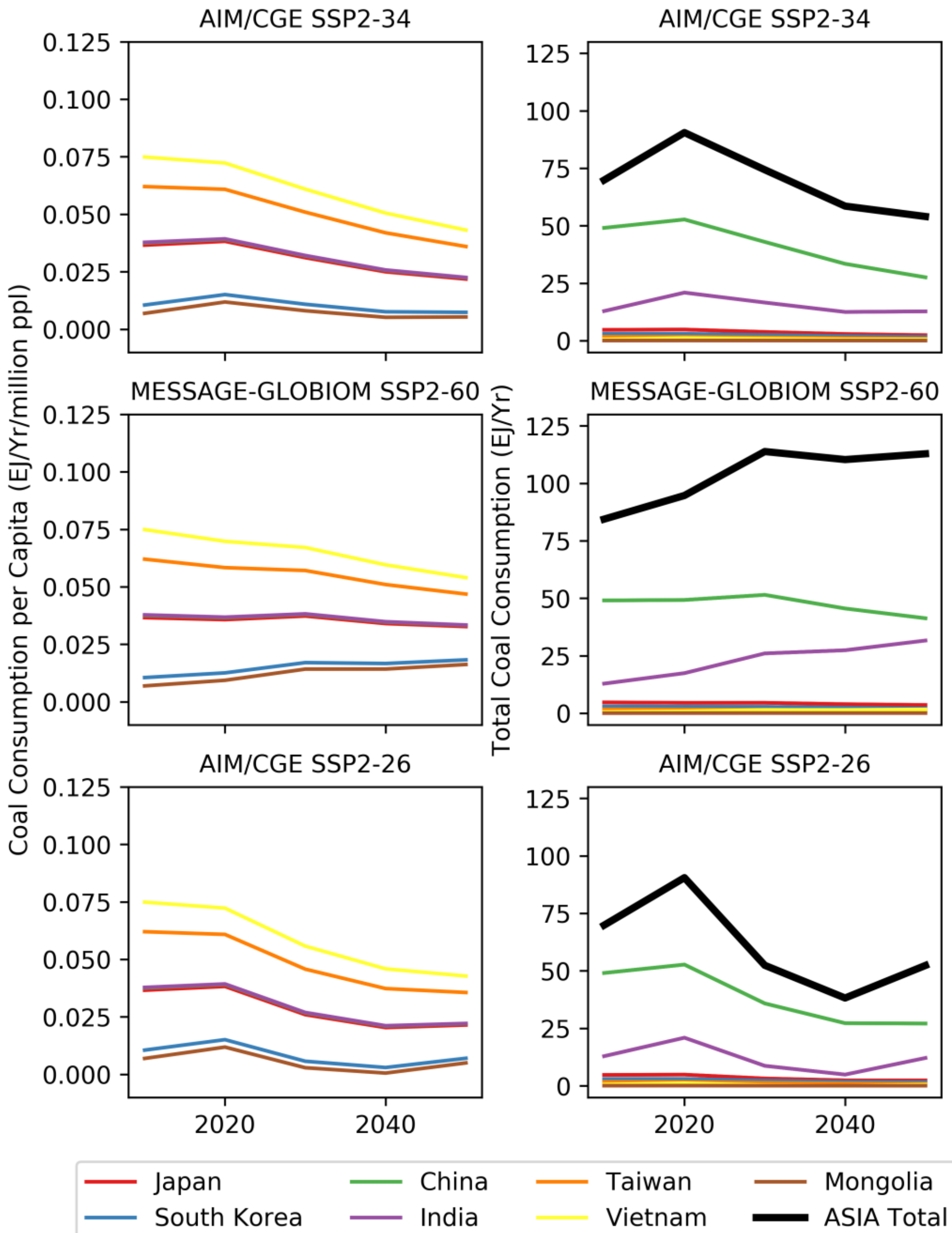

Figure S27. Future per Million Capita Coal Consumption (EJ/Yr/million) and Future Total Coal Consumption (EJ/Yr) for Selected Countries Downscaled Using Linear Convergence. Additional comparison is made between the future country-level and ASIA-level total coal consumptions.

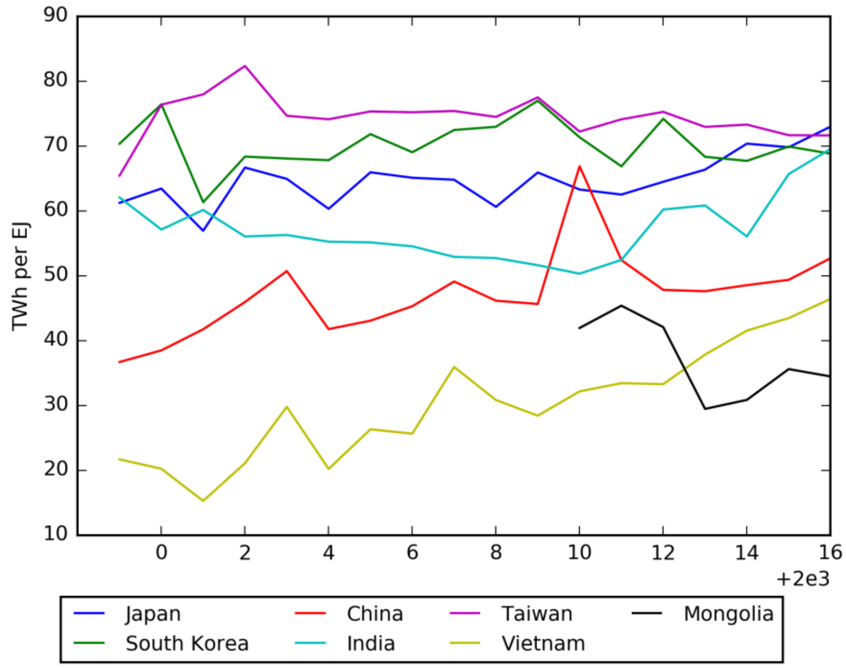

Figure S28. Historical Conversion Factors between Coal Consumption and Electricity Generation ($h_{j,t}$) for Selected Countries. Data source: International Energy Agency.[68,72]

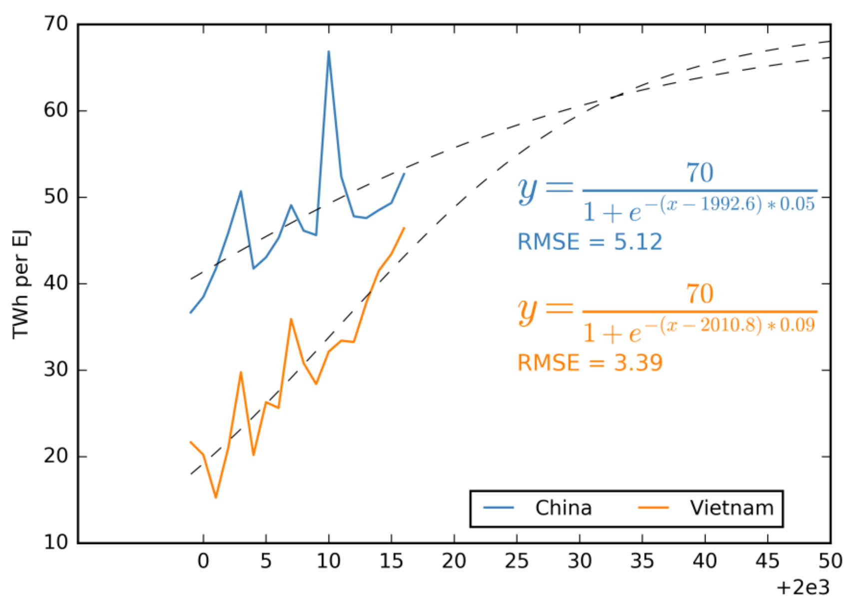

Figure S29. Fitted Logistic Trend Lines for the Historical Conversion Factors between Coal Consumption and Electricity Generation ($h_{j,t}$) for China and Vietnam.[68,72] RMSE: root mean square errors of the fit.

Table S12. Historical Average Capacity Factors of Coal-Fired Power Plants in the States of India, Provinces of China, and Other Countries.

Country	Average Capacity Factor	Reporting Year
Bangladesh[6]	0.387	Fiscal Year 2016
Cambodia[7]	0.603	2015
China[15]γ	0.446	2016
India[16]	0.520	2016
Japan[73]	0.44	
Laos[8]α	0.996	2016
Mongolia[9]	0.645	2014
Myanmar[10,11]	0.114	2014
Pakistan[12]β	0.116	2015
South Korea[13]	0.900	2015
Taiwan[73]ε	0.47	Unknown
Thailand[14]β	0.752	2016
Vietnam[12]β	0.399	2015

α Only one coal-fired power plant (Hongsa) exists in Laos. Units 1&2 began operation at the end of 2015 and unit 3 began operation in 2016. We used the target total net generation for 2016 for unit 1&2 to calculate an approximate capacity factor.
β Because the data source only has electricity generation, we calculated capacity factor by dividing the electricity generation by the total installed capacity until the reporting year in the GCPT17 dataset[1].
γ The data did not distinguish between fuels for thermoelectric generation, and thus contains a small part of natural gas power plants.
ε No data is available for Taiwan. Therefore, the 'other non-OECD Asia' entry is used.

The downscaled national level coal capacity and comparison to the total existing and planned coal capacity in the GCPT17 dataset[67] are shown in Table S13. When the downscaled capacities are smaller, it indicates that more plants have been identified as in planning than are actually projected by the IAM. This would be expected as not all plants pass through the planning stage. In the few cases where the downscaled capacities are greater (Bangladesh, Pakistan and Myanmar), it indicates that the downscaled scenario has more power plants than are currently planned by 2030 in the country. In these negative cases, we set the downscaled capacities to be equal the GCPT17 capacities, i.e. retaining all existing and planned coal-fired power plants in GCPT17 but not making up any new ones.

Table S13. The Downscaled Coal-Fired Capacity at Country Level for Various ASIA Regional Scenarios, and the Existing + Planned Coal-Fired Capacities at Country Level in the GCPT17[67] Dataset. Unit: MW. The ASIA regional scenarios are the same as in Figure S25.

	Downscaled			GCPT17
	AIM/CGE SSP2-34	MESSAGE-GLOBIOM SSP2-60	AIM/CGE SSP2-26	
China	401056	600833	394172	1004504

India	187905	465243	178349	327335
Japan	574	853	564	780
Mongolia	517	767	508	9486
South Korea	8590	11187	8500	27778
Taiwan	8705	10901	8629	11604
Vietnam	8070	24455	7505	36202
Bangladesh	29599	73285	28094	7070
Pakistan	144166	356948	136835	12695
Cambodia	1021	3094	950	1310
Laos	361	1093	335	1878
Myanmar	17755	53805	16513	710
Thailand	2474	7497	2301	5629

6.3 Local Installed Coal Capacity

We further refined the downscaled national level coal capacities from section 6.2 ($C_{j,t}$, after the scaling down to the coverage of the hydrological data, and after removing the negative values) for China and India, because these two countries are large and cover diverse wet and dry regions. This step used proportional downscaling, as in Eq. (S6):

$$C_{j,t,c} = \frac{E_{j,c} + N_{j,c}}{E_j + N_j} C_{j,t} \tag{S6}$$

, where the subscript c means a province of China or a state of India, E_j and $E_{j,c}$ are the existing coal capacity of country j (China or India) or province/state c, N_j and $N_{j,c}$ are the planned coal capacity of country j (China or India) or province/state c.

In the final step, we used random sampling to convert the national- ($C_{j,t}$) and state-level ($C_{j,t,c}$) capacities to binary decisions for each power plant. For each existing or planned coal-fired power plant in the GCPT17 dataset,[67] we kept the power plant with a probability inversely proportional to its age by 2050, i.e. Eq. (S7), so that older power plants were more likely to be eliminated:

$$p_{1k} = a_j \text{ or } a_{j,c} \frac{1}{2050 - Y_k} \tag{S7}$$

, where p_{1k} is the probability of keeping a power plant k, Y_k is the year that the power plant entered/expects to enter operation, and a_j or $a_{j,c}$ is a normalizing coefficient that is chosen for the country j or province/state

c to satisfy Eq. (S8), i.e. the expected amount of kept capacity is equal to the downscaled national or province/state-level capacity:

$$C_{j,t} \text{ or } C_{j,t,c} = \sum_{k \in R_j \text{ or } R_{j,c}} p_{1k} M_k \tag{S8}$$

, where R_j ($R_{j,c}$) are the set of coal-fired power plants in country j (province/state c), and M_k is the nameplate capacity of power plant k.

We conducted the random sampling 1000 times on the whole region, and kept the three samples that are most similar to the downscaled pattern of $C_{j,t}$'s and $C_{j,t,c}$'s, using the sum of absolute percentage differences (R_1) defined by Eq. (S9):

$$R_1 = \sum_{j \in (W_o \setminus W_1)} \frac{\left|C_{j,t}^s - C_{j,t}\right|}{C_{j,t}} + \sum_{j \in W_1} \sum_{c \in W_j} \frac{\left|C_{j,t,c}^s - C_{j,t,c}\right|}{C_{j,t,c}} \tag{S9}$$

, where the superscript s denotes random sampling, W_o is the set of all countries in the study region, W_1 is the set {China, India}, W_j is the set of provinces/states of country j.

During the random sampling, we found 54 operating coal-fired power plants in GCPT17 that do not report the year of entering operation. We set the Y_k of these power plants to be the average Y_t of the other operating coal-fired power plants. The normalized probability of keeping a power plant was also greater than 1 in some cases, and we simply set the probability to 1, which did not prevent the random sampling from achieving consistency with the national level downscaled scenarios (Table S14). The only large difference between the national scenarios and the random samples occurred for Laos, which is because the country only has three power generation units in GCPT17,[67] and addition/subtraction operations between their capacity values cannot give rise to values that are similar to the Laos national scenarios (Table S13).

Table S14. Relative Differences between the Downscaled National Coal-Fired Electricity Generation Capacities and the Actual National Total Capacities in the Random Samples. Unit: %.

Scenario	AIM/CGE SSP2-34			MESSAGE-GLOBIOM SSP2-60			AIM/CGE SSP2-26		
Sample	1	2	3	1	2	3	1	2	3
China	0.01	0.01	-0.04	0.00	-0.01	-0.01	0.00	0.00	0.00
India	0.01	0.03	0.01	0.00	0.00	0.00	-0.02	-0.01	-0.02
Japan	-8.74	-8.74	-8.74	0.00	0.00	0.00	-10.59	-10.59	-10.59
Mongolia	-2.52	-2.52	-2.52	0.88	-1.73	-1.73	1.64	1.64	1.64
South Korea	-0.02	0.05	-0.12	0.00	0.02	0.04	0.08	0.01	-0.11
Taiwan	-0.02	-0.03	-0.10	0.00	0.03	-0.05	-0.12	0.02	0.13
Vietnam	0.04	0.04	0.06	-0.01	-0.05	-0.06	0.04	0.00	0.08
Bangladesh	0.00	0.00	0.00	0.00	0.00	0.00	0.00	0.00	0.00
Pakistan	0.00	0.00	0.00	0.00	0.00	0.00	0.00	0.00	0.00
Cambodia	-1.86	-1.86	-1.86	0.00	0.00	0.00	4.70	4.70	4.70
Laos	-73.56	-73.56	-73.56	-14.54	-14.54	-14.54	-86.61	-86.61	-86.61
Myanmar	0.00	0.00	0.00	0.00	0.00	0.00	0.00	0.00	0.00
Thailand	0.04	-0.16	-0.16	0.00	0.00	0.00	-0.05	0.04	-0.18

6.4 Local Scenarios of CO_2 Capture and Storage (CCS) Deployment

There are few existing CCS power plants in the study region for inferring potential future deployment of CCS power plants. Therefore, we used random sampling to decide whether to retrofit an existing/equip a planned coal-fired power plant with CCS. CCS is water-intensive and thus less likely to be deployed in the water-stressed parts of the study region; also, the efficiency concerns of CCS makes it less likely to be deployed on the older power plants. Therefore, we set the probability of retrofitting an existing/equipping a planned coal-fired power plant with CCS to be a weighted sum of two parts, i.e. Eq. (S10):

$$p_{2k} = \frac{a_2}{2050 - Y_k} + \frac{b_2 Q_k^{0.1}}{M_k} \tag{S10}$$

, where p_{2k} is the probability that power plant k uses CCS, Q_k is the annual mean streamflow (under the 1.5°C, 2°C, or 3°C scenario, averaged over all the GCMs) in the grid cell of the location of power plant k, and the normalizing coefficients a_2 and b_2 are chosen to satisfy Eq. (S11) and Eq. (S12), so that the expected amount of coal capacity with CCS is equal to the regional scenario:

$$0.5 * fC = \sum_{j \in W_o} \sum_{k \in R_j} \frac{a_2}{2050 - Y_k} M_k \tag{S11}$$

$$0.5 * fC = \sum_{j \in W_o} \sum_{k \in R_j} b_2 Q_k^{0.1} \tag{S12}$$

, where f is the fraction of coal consumption that is fitted with CCS (Figure S25), C is the total kept capacity of coal-fired power plants in the study region during the random sampling of section 6.3. The exponent 0.1 in Eq. (S10) and Eq. (S12) reduces the disparity between streamflow at different locations. Otherwise, normalization by b_2 leads to a considerable portion of p_{2k} being greater than one, i.e. unable to function as a probability.

We conducted the random sampling 1000 times on the whole region, and for each set of kept power plants from section 6.3, we kept the three sample sets that have the most similar level of CCS deployment to the regional scenarios (Figure S25), with the level similarity being measured by Eq. (S13):

$$R_2 = |D^s - fC| \tag{S13}$$

, where D^s is the randomly sampled coal capacity that are fitted with CCS.

Table S15 compares the fraction of coal consumption with CCS in the regional scenarios (Figure S25) and the fraction of coal-fired generation capacity with CCS obtained from random sampling. For the AIM/CGE SSP2-26 scenario, which corresponds to 1.5°C warming and has high level of CCS deployment, the sampled levels of CCS deployment were always lower, but reducing the exponent in Eq. (S10) and Eq. (S12) down to $1*10^{-5}$ did not considerably reduce the gap. Since the downscaled scenarios in general are illustrative in nature, and cannot follow any real world pathways due to their simplistic assumptions, we consider this level of gap to be acceptable.

Table S15. Target versus Sampled Levels of CCS Deployment, i.e., the Fraction of Coal Consumption Fitted with CCS in the ASIA Regional SSP2 Scenario and the Fractions of Coal-Fired Generation with CCS Capacity in the Random Sampled Results. Note: the AIM/CGE SSP2-34 scenario, which correspond to 3^{o}C warming above pre-industrial levels, do not have any CCS deployment.

	Scenario	**AIM/CGE SSP2-26**			**AIM/CGE SSP2-34**		
	Original SSP2 Scenario			0.5432			0.8071
	Power Plant Sample	1	2	3	1	2	3
CCS Sample	1	0.5431	0.5433	0.5433	0.776	0.7658	0.7638
	2	0.5429	0.5426	0.5431	0.7677	0.7647	0.7637
	3	0.5438	0.5426	0.5429	0.7636	0.7645	0.762

Figure S30 through Figure S32 show the spatial distributions of the coal-fired power plants that are operational and using or not using CCS in the final nine random samples. In all random samples, the power plants and CCS deployments are dispersed in space.

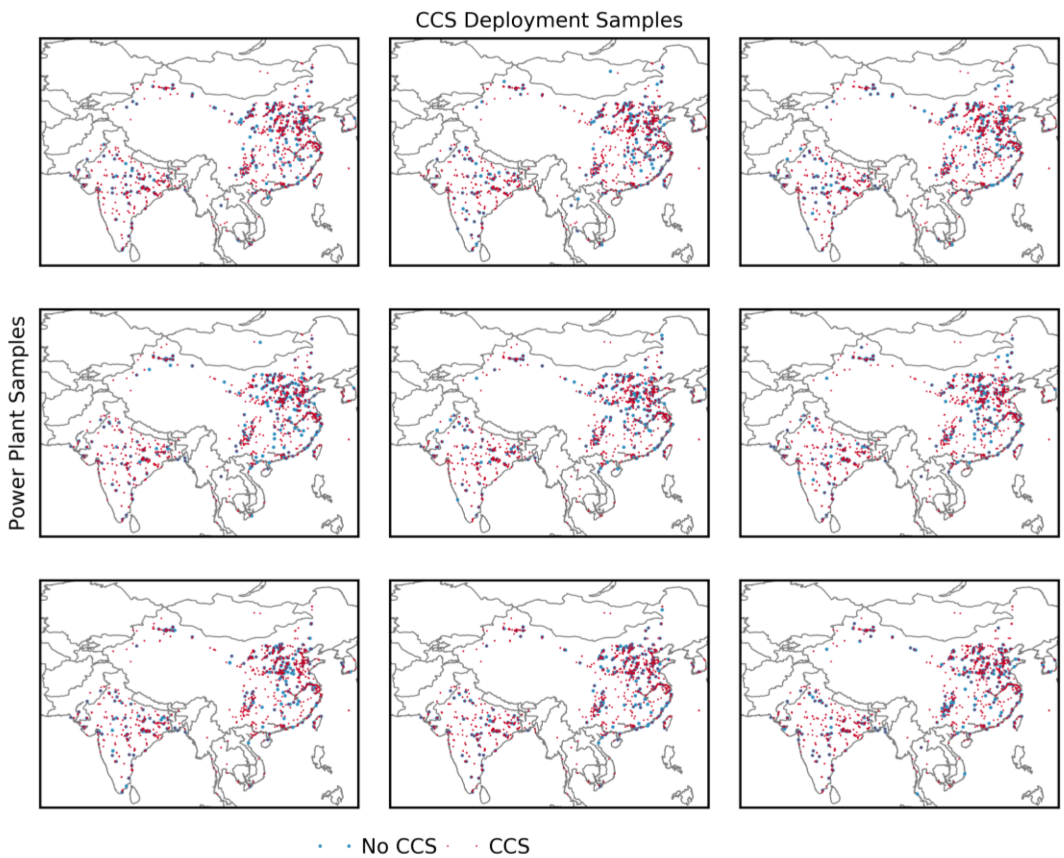

Figure S30. Downscaled Locations of Coal Power Plants and CCS Deployment from the AIM-CGE SSP2-26 Scenario for ASIA. Each row belong to the same sample of power plant locations, upon which three more samples of CCS deployment were constructed.

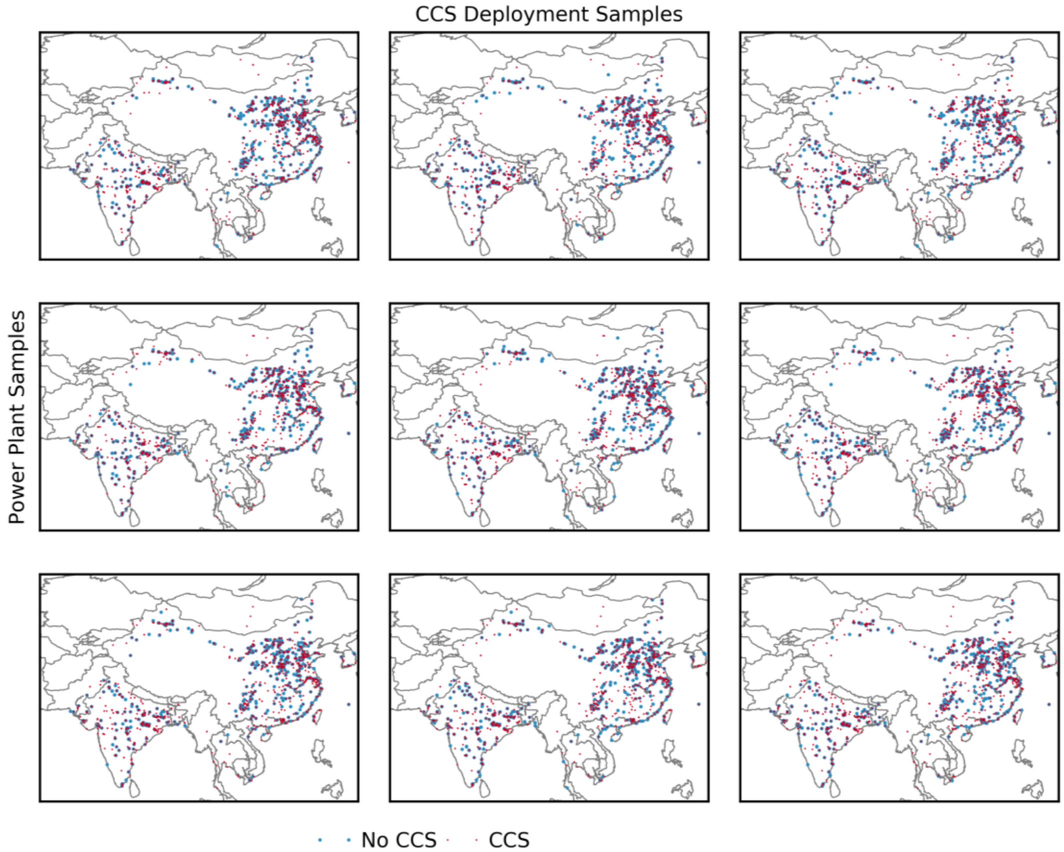

Figure S31. Downscaled Locations of Coal Power Plants and CCS Deployment from the AIM-CGE SSP2-34 Scenario for ASIA. Each row belong to the same sample of power plant locations, upon which three more samples of CCS deployment were constructed.

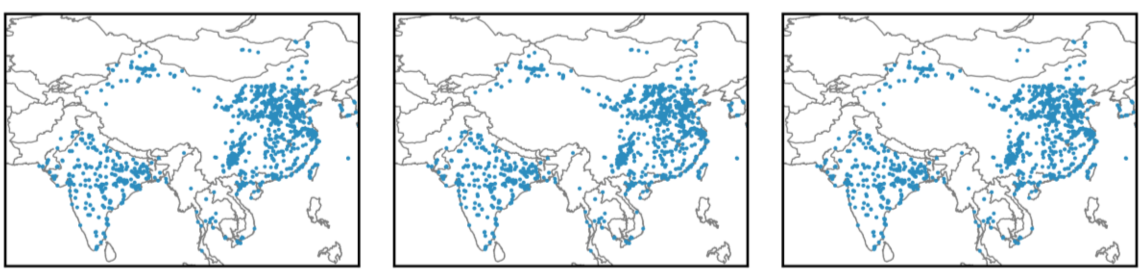

Figure S32. Downscaled Locations of Coal Power Plants and CCS Deployment from the MESSAGE-GLOBIOM SSP2-60 Scenario for ASIA. Each row belong to the same sample of power plant locations, upon which three more samples of CCS deployment were constructed.

7 The Energy Penalty of Dry Cooling Relative to Cooling Towers

With the same net electricity generation, dry-cooled thermal power plants consume more fuel than water-cooled plants because (1) the steam turbine has higher backpressure and therefore lower efficiency, and (2) the operation of fans for dry cooling consumes more energy than the operation of pumps for once-through cooling systems and natural-draft wet cooling towers, and the operation of both fans and pumps for mechanical- and induced-draft wet cooling towers.[74] We used an approach developed by the U.S. Environmental Protection Agency to calculate (1) and (2) because the formulas are developed based on empirical data, require minimal inputs, and reflect the impact of air temperature – which differs greatly between the north and south of our study region – on the energy penalty.[74] This approach is summarized below.

Change in the efficiency of the steam turbine from the efficiency under design conditions ($\Delta\eta$) is a function of turbine backpressure (p, 10^4 Pa). Eq. (S14) shows this function when the turbine is operating at maximum steam load, which we assume is applicable in the summer months (June-July-August). Eq. (S15) shows this function for 67% steam load, which we assume is applicable during the rest of the year (September-May).

$$\Delta\eta = -0.0129p^3 + 0.0706p^2 - 0.0472p + 0.0078 \tag{S14}$$

$$\Delta\eta = 0.0549p^2 - 0.0118p - 0.0062 \tag{S15}$$

For wet cooling towers, the turbine backpressure (p) is a function of the condenser inlet temperature, equal to the sum of ambient wet-bulb temperature (T_{wb}, ºC) and tower approach (T_{app}, ºC), as shown in Eq. (S16):

$$p = 0.4591 \exp\left[0.03834\left(T_{wb} + T_{app} + 35.56\right)\right] \tag{S16}$$

For dry cooling, the turbine backpressure (p) is a function of the ambient air temperature (T_{air}, ºC), as shown in Eq. (S17):

$$p = 1.031 \exp\left(0.0306\left(T_{air} + 32\right)\right) \tag{S17}$$

The loss of thermal efficiency at power-plant level due to the operation of fans and pumps for cooling towers depends on the tower approach (T_{app}), distance between the water source and the power plant, and diameter of water pipes, but a rule of thumb value is 1.18% of the net electricity generation.[74] The loss of thermal efficiency at power-plant level due to the operation of fans for dry cooling is about 2.43% of the net electricity generation.[74] With these values, Eq. (S14), and Eq. (S17), one can calculate the energy penalty of switching from wet cooling tower to dry cooling as ($\Delta\eta^{dry}$+2.43%)-($\Delta\eta^{tower}$+1.18%), where the superscripts *dry* and *tower* indicates dry cooling and cooling tower.

References

[1] Endcoal, Plant Tracker - Frequently Asked Questions, http://endcoal.org/global-coal-plant-tracker/about-the-tracker/.

[2] C. E. Raptis, M. T. H. van Vliet and S. Pfister, Global Thermal Pollution of Rivers from Thermoelectric Power Plants, *Environmental Research Letters*, 2016, **11**, 104011.

[3] C. E. Raptis and S. Pfister, Global Freshwater Thermal Emissions from Steam-Electric Power Plants with Once-Through Cooling Systems, *Energy*, 2016, **97**, 46–57.

[4] International Organization for Standardization, ISO 3166-1:2013, https://www.iso.org/standard/63545.html, (accessed 26 June 2019).

[5] International Organization for Standardization, ISO 3166-2:2013, https://www.iso.org/standard/63546.html, (accessed 26 June 2019).

[6] Bangladesh Power Development Board, *Annual Report 2015-16*, 2016.

[7] Electricity Authority of Cambodia, *Report on Power Sector of the Kingdom of Cambodia*, 2016.

[8] Department of Energy Policy and Planning, Hongsa Power Company Limited, http://www.laoenergy.la/pageMenu.php?id_menu=47.

[9] International Renewable Energy Agency, *Mongolia Renewables Readiness Assessment*, 2016.

[10] Myanmnar Statistical Information Service, Electricity Power Generation by Type and Location, http://www.mmsis.gov.mm/sub_menu/statistics/search.jsp.

[11] Myanmnar Statistical Information Service, Electricity Power Installation by Type and Location, http://www.mmsis.gov.mm/sub_menu/statistics/search.jsp.

[12] International Energy Agency, Statistics Search Report (Topic: Electricity and Heat), http://www.iea.org/statistics/statisticssearch/.

[13] Korea Energy Economics Institute, *Yearbook of Energy Statistics 2016*, 2016.

[14] Energy Policy and Planning Office of Ministry of Energy, Energy Statistics - Electricity, http://www.eppo.go.th/index.php/en/en-energystatistics/electricity-statistic?orders[publishUp]=publishUp&issearch=1.

[15] North Star Electricity News Center, 2016 Province Wise Thermoelectric Generation Capacity and Utilization Hours, http://news.bjx.com.cn/html/20170207/806749.shtml.

[16] Central Electricity Authority, *Monthly Reports - Generation Reports - Generation Overview Report - Actual - Region Wise State Wise and Station Wise Details*, 2016.

[17] M. D. Bartos and M. V. Chester, Impacts of Climate Change on Electric Power Supply in the Western United States, *Nature Climate Change*, 2015, **5**, 748–752.

[18] M. J. Rutberg, Modeling Water Use at Thermoelectric Power Plants, Massachusetts Institute of Technology, 2012.

[19] T. H. Diehl, M. A. Harris, J. C. Murphy, S. S. Hutson and D. E. Ladd, *Methods for Estimating Water Consumption for Thermoelectric Power Plants in the United States*, 2013.

[20] A. D. Martín, Water Footprint of Electric Power Generation: Modeling Its Use and Analyzing Options for a Water-Scarce Future, Massachusetts Institute of Technology, 2012.

[21] C. Zhang, L. D. Anadon, H. Mo, Z. Zhao and Z. Liu, Water − Carbon Trade-off in China's Coal Power Industry, *Environmental Science & Technology*, 2014, **48**, 11082–11089.

[22] X. Liang, Z. Wang, Z. Zhou, Z. Huang, J. Zhou and K. Cen, Up-To-Date Life Cycle Assessment and Comparison Study of Clean Coal Power Generation Technologies in China, *Journal of Cleaner Production*, 2013, **39**, 24–31.

[23] National Energy Technology Laboratory, *Cost and Performance Baseline for Fossil Energy Plants Volume 1: Bituminous Coal and Natural Gas to Electricity*, 2013.

[24] International Energy Agency, *Regional Trends in Energy-Efficient, Coal-Fired, Power Generation Technologies*, 1998.

[25] National Energy Technology Laboratory, *Cost and Performance Baseline for Fossil Energy Plants Volume 3b Low Rank Coal to Electricity Combustion Cases*, 2011.

[26] State Economic and Trade Commission, Electricity Industry Standard of the People's Republic of China - Guide for Water Saving of Thermal Power Plant (DL/ T783-2001), 2002, 1–14.

[27] Socialist Republic of Vietnam, *National Technical Regulation on Industrial Wastewater (QCVN 24:2009/BTNMT) (in Vietnamese)*, 2009.

[28] The Environmental Protection Department, *Effluent Standard (in Traditional Chinese)*, Taiwan, 2014.

[29] China Electric Power Enterprise Federation, GB 50660-2011 Code for Design of Fossil Fired Power Plant (in Chinese), 2012, 1–368.

[30] Central Pollution Control Board, [Schedule - VI] General Standards for Discharge of Environmental Pollutants Part A: Effluents, in *The Environment (Protection) Rules, 1986*, 1986, pp. 545–560.

[31] T. H. Diehl and M. A. Harris, *Withdrawal and Consumption of Water by Thermoelectric Power Plants in the United States, 2010: U.S. Geological Survey Scientific Investigations Report 2014–5184*, 2014.

[32] National Energy Technology Laboratory, *Quality Guidelines for Energy System Studies - Detailed Coal Specifications (DOE/NETL-401/012111)*, 2012.

[33] S. Su, B. Li, S. Cui and S. Tao, Sulfur Dioxide Emissions from Combustion in China from 1990 to 2007, *Environmental Science and Technology*, 2011, **45**, 8403–8410.

[34] S. Jayanti, K. Maheswaran and V. Saravanan, Assessment of the Effect of High Ash Content in Pulverized Coal Combustion, *Applied Mathematical Modelling*, 2007, **31**, 934–953.

[35] Central Electricity Authority, *CO_2 Baseline Database for the Indian Power Sector User Guide (Version 9.0)*, 2014.

[36] Coal Controller's Organization, *Coal Directory of India 2013-14 Coal Statistics*, Kolkata, India, 2014.

[37] Coal Controller's Organization, *Provisional Coal Statistics 2015-16*, Kolkata, India, 2016.

[38] Ministry of Coal, Coal Grades, http://coal.nic.in/content/coal-grades.

[39] Ministry of Coal, Category of Coal, http://pib.nic.in/newsite/PrintRelease.aspx?relid=108242.

[40] H. Yang and M. Pollitt, Incorporating Both Undesirable Outputs and Uncontrollable Variables into DEA: The Performance of Chinese Coal-Fired Power Plants, *European Journal of Operational Research*, 2009, **197**, 1095–1105.

[41] Y. Zhao, S. Wang, L. Duan, Y. Lei, P. Cao and J. Hao, Primary Air Pollutant Emissions of Coal-Fired Power Plants in China: Current Status and Future Prediction, *Atmospheric Environment*, 2008, **42**, 8442–8452.

[42] Central Electricity Authority, *Standard Design Criteria/Guidelines for Balance of Plant of 2x(500MW or Above) Thermal Power Project*, New Delhi, India, 2010.

[43] C. Zhang, L. Zhong, X. Fu, J. Wang and Z. Wu, Revealing Water Stress by the Thermal Power

Industry in China Based on a High Spatial Resolution Water Withdrawal and Consumption Inventory, *Environmental Science & Technology*, 2016, **50**, 1642–1652.

[44] A. Bhattacharya and B. K. Mitra, *Water Availability for Sustainable Energy Policy Assessing cases in South and South East Asia*, Hayama, Japan, 2013.

[45] Centre for Science and Environment, *The State of our Power Plants - Green Rating of Coal-based Thermal Power Sector*, 2015.

[46] E. H. Sutanudjaja, R. van Beek, N. Wanders, Y. Wada, J. H. C. Bosmans, N. Drost, R. J. van der Ent, I. E. M. de Graaf, J. M. Hoch, K. de Jong, D. Karssenberg, P. López López, S. Peßenteiner, O. Schmitz, M. W. Straatsma, E. Vannametee, D. Wisser and M. F. P. Bierkens, PCR-GLOBWB 2: a 5arcmin Global Hydrological and Water Resources Model, *Geoscientific Model Development*, 2018, **11**, 2429–2453.

[47] National Institute of Ecology, *Environmental Flows An Introduction for Water Resources Managers*, New Delhi, 2013.

[48] A. Chen, X. Sui, W. Liao and K. Chen, Review Study on Instream Ecological Base Flow in China (In Chinese), *Journal of China Institute of Water Resources and Hydropower Research*, 2016, **14**, 401–411.

[49] P. Nilsalab, S. H. Gheewala and T. Silalertruksa, Methodology Development for Including Environmental Water Requirement in the Water Stress Index Considering the Case of Thailand, *Journal of Cleaner Production*, 2018, **167**, 1002–1008.

[50] N. L. Poff, B. D. Richter, A. H. Arthington, S. E. Bunn, R. J. Naiman, E. Kendy, M. Acreman, C. Apse, B. P. Bledsoe, M. C. Freeman, J. Henriksen, R. B. Jacobson, J. G. Kennen, D. M. Merritt, J. A. Y. H. O'Keeffe, J. D. Olden, K. Rogers, R. E. Tharme and A. Warner, The Ecological Limits of Hydrologic Alteration (ELOHA): A New Framework for Developing Regional Environmental Flow, *Freshwater Biology*, 2010, **55**, 147–170.

[51] C. J. Gippel, N. R. Bond, C. James and X. Wang, An Asset-based, Holistic, Environmental Flows Assessment Approach, *International Journal of Water Resources Development*, 2009, **25**, 301–330.

[52] A. V Pastor, F. Ludwig, H. Biemans, H. Hoff and P. Kabat, Accounting for Environmental Flow Requirements in Global Water Assessments, *Hydrology and Earth System Sciences*, 2014, **18**, 5041–5059.

[53] K. M. Salik, M. Z. ur R. Hashmi, S. Ishfaq and W. ul Z. Zahdi, Environmental Flow Requirements and Impacts of Climate Change-Induced River Flow Changes on Ecology of the Indus Delta, Pakistan, *Regional Studies in Marine Science*, 2016, **7**, 185–195.

[54] V. Smakhtin and M. Anputhas, *An Assessment of Environmental Flow Requirements of Indian River Basins (Research Report 107)*, Colombo, Sri Lanka, 2006.

[55] A. Schröder, F. Kunz, J. Meiss, R. Mendelevitch and C. von Hirschhausen, *Current and Prospective Costs of Electricity Generation until 2050 (Data Documentation)*, Berlin, Germany, 2013.

[56] National Bureau of Statistics of China, Annual Data by Province - Thermoelectric Generation (in Chinese), http://data.stats.gov.cn/easyquery.htm?cn=E0103.

[57] H. Fan, Z. Duan and W. Shan, The Developmenet of Gas-Fired Power in China: Current Status and Prospect (in Chinese), *Energy of China*, 2015, **2**, 37–42.

[58] International Institute for Applied Systems Analysis, SSP Database (Shared Socioeconomic Pathways) - Version 1.1, https://tntcat.iiasa.ac.at/SspDb/dsd?Action=htmlpage&page=about.

[59] D. P. van Vuuren, S. J. Smith and K. Riahi, Downscaling Socioeconomic and Emissions Scenarios for Global Environmental Change Research: A Review, *Wiley Interdisciplinary Reviews: Climate Change*, 2010, **1**, 393–404.

[60] S. Fujimori, M. Abe, T. Kinoshita, T. Hasegawa, H. Kawase, K. Kushida, T. Masui, K. Oka, H. Shiogama, K. Takahashi, H. Tatebe and M. Yoshikawa, Downscaling Global Emissions and Its Implications Derived from Climate Model Experiments, *PLoS ONE*, 2017, **12**, 1–20.

[61] D. P. van Vuuren, P. L. Lucas and H. Hilderink, Downscaling Drivers of Global Environmental Change: Enabling Use of Global SRES Scenarios at the National and Grid Levels, *Global*

Environmental Change, 2007, **17**, 114–130.

[62] A. S. Kebede, R. J. Nicholls, A. Allan, I. Arto, I. Cazcarro, J. A. Fernandes, C. T. Hill, C. W. Hutton, S. Kay, A. N. Lázár, I. Macadam, M. Palmer, N. Suckall, E. L. Tompkins, K. Vincent and P. W. Whitehead, Applying the Global RCP–SSP–SPA Scenario Framework at Sub-National Scale: A Multi-Scale and Participatory Scenario Approach, *Science of the Total Environment*, 2018, **635**, 659–672.

[63] B. Frame, J. Lawrence, A. G. Ausseil, A. Reisinger and A. Daigneault, Adapting Global Shared Socio-Economic Pathways for National and Local Scenarios, *Climate Risk Management*, 2018, **21**, 39–51.

[64] A. Grübler, B. O'Neill, K. Riahi, V. Chirkov, A. Goujon, P. Kolp, I. Prommer, S. Scherbov and E. Slentoe, Regional, National, and Spatially Explicit Scenarios of Demographic and Economic Change Based on SRES, *Technological Forecasting and Social Change*, 2007, **74**, 980–1029.

[65] T. O. West, Y. Le Page, M. Huang, J. Wolf and A. M. Thomson, Downscaling Global Land Cover Projections from an Integrated Assessment Model for Use in Regional Analyses: Results and Evaluation for the US from 2005 to 2095, *Environmental Research Letters*, 2014, **9**, 064004.

[66] G. C. Hurtt, L. P. Chini, S. Frolking, R. A. Betts, J. Feddema, G. Fischer, J. P. Fisk, K. Hibbard, R. A. Houghton, A. Janetos, C. D. Jones, G. Kindermann, T. Kinoshita, K. Klein Goldewijk, K. Riahi, E. Shevliakova, S. Smith, E. Stehfest, A. Thomson, P. Thornton, D. P. van Vuuren and Y. P. Wang, Harmonization of Land-Use Scenarios for the Period 1500-2100: 600 Years of Global Gridded Annual Land-Use Transitions, Wood Harvest, and Resulting Secondary Lands, *Climatic Change*, 2011, **109**, 117–161.

[67] CoalSwarm, Global Coal Plant Tracker, http://endcoal.org/tracker/.

[68] International Energy Agency, *Coal Information 2018*, OECD Publishing, Paris, France, 2018.

[69] National Statistics Republic of China (Taiwan), 02. Population and Housing, https://eng.stat.gov.tw/ct.asp?xItem=41871&ctNode=6339&mp=5.

[70] The World Bank, Population, Total, https://data.worldbank.org/indicator/sp.pop.totl, (accessed 27 June 2019).

[71] B. J. and B. C. O'Neill, Spatially Explicit Global Population Scenarios Consistent with the Shared Socioeconomic Pathways, *Environmental Research Letters*, 2016, **11**, 84003.

[72] International Energy Agency, *Electricity Information 2018*, OECD Publishing, Paris, France, 2018.

[73] Energy Information Administration, Electric Generator Capacity Factors Vary Widely Across the World, https://www.eia.gov/todayinenergy/detail.php?id=22832.

[74] Environmental Protection Agency, *Technical Development Document for the Final Regulations Addressing Cooling Water Intake Structures for New Facilities (EPA-821-R-01-036)*, 2001.